OPEN ACCESS Freely available online

PLOS ONE

Speeding Up Social Waves. Propagation Mechanisms of Shimmering in Giant Honeybees

Gerald Kastberger[1]*, Thomas Hoetzl[1], Michael Maurer[2], Ilse Kranner[3], Sara Weiss[1], Frank Weihmann[1]

1 Institute of Zoology, University of Graz, Graz, Austria, **2** Institute for Computer Graphics and Vision, Graz University of Technology, Graz, Austria, **3** Institute of Botany, University of Innsbruck, Innsbruck, Austria

Abstract

Shimmering is a defence behaviour in giant honeybees (*Apis dorsata*), whereby bees on the nest surface flip their abdomen upwards in a Mexican wave-like process. However, information spreads faster than can be ascribed to bucket bridging, which is the transfer of information from one individual to an adjacent one. We identified a saltatoric process that speeds up shimmering by the generation of daughter waves, which subsequently merge with the parental wave, producing a new wave front. Motion patterns of individual "focus" bees (n = 10,894) and their shimmering-active neighbours (n = 459,558) were measured with high-resolution video recording and stereoscopic imaging. Three types of shimmering-active surface bees were distinguished by their communication status, termed "agents": "Bucket-bridging" agents comprised 74.98% of all agents, affected 88.17% of their neighbours, and transferred information at a velocity of $v = 0.317 \pm 0.015$ m/s. "Chain-tail" agents comprised 9.20% of the agents, were activated by 6.35% of their neighbours, but did not motivate others to participate in the wave. "Generator agents" comprised 15.82% of agents, showed abdominal flipping before the arrival of the main wave front, and initiated daughter waves. They affected 6.75% of their neighbourhood and speeded up the compound shimmering process compared to bucket bridging alone by 41.5% to $v = 0.514 \pm 0.019$ m/s. The main direction of shimmering was reinforced by 35.82% of agents, whereas the contribution of the complementing agents was fuzzy. We discuss that the saltatoric process could enable the bees to instantly recruit larger cohorts to participate in shimmering and to respond rapidly to changes in flight direction of preying wasps. A third, non-exclusive explanation is that at a distance of up to three metres from the nest the acceleration of shimmering could notably contribute to the startle response in mammals and birds.

Citation: Kastberger G, Hoetzl T, Maurer M, Kranner I, Weiss S, et al. (2014) Speeding Up Social Waves. Propagation Mechanisms of Shimmering in Giant Honeybees. PLoS ONE 9(1): e86315. doi:10.1371/journal.pone.0086315

Editor: Anna Dornhaus, University of Arizona, United States of America

Received June 19, 2013; **Accepted** December 6, 2013; **Published** January 27, 2014

Funding: Funding for the paper was granted by the Austrian Science Fund (FWF Project P 20515-B16, entitled "Social waves in giant honeybees"). The funders had no role in study design, data collection and analysis, decision to publish, or preparation of the manuscript.

Competing Interests: The authors have declared that no competing interests exist.

* E-mail: gerald.kastberger@uni-graz.at

Introduction

Shimmering [1–9] in giant honeybees (*Apis dorsata*) is one of the most sophisticated communication behaviours in insects. Shimmering takes place at the nest surface [1,3–9], which constitutes a matrix of densely clustered individuals arranged in a multi-layered stratum, forming the *bee curtain* [10] around a central, flat comb (Fig. 1A). In shimmering, individual bees flip their abdomens upwards, producing wave-like patterns (Movies S1, S2, S3, S4, S5, S6), which propagate across the nest surface in about one second, also affecting sub-surface layers [7–8]. Giant honeybees show this collective behaviour in response to threatening enemies, in particular to predatory wasps [6]. It is commonly accepted that colony defence is the primary goal of shimmering [6,11–12].

Some of the mechanisms of shimmering have been clarified [6–9,11–14], but it is not fully understood how the waves propagate [7–9]. Shimmering has been described as a Mexican-wave-like process [15], following the principles of *bucket-bridging* [7,9] to transfer information along a chain of agents, such as passing a bucket of water from one person to another to extinguish a fire in the old days. The *bucket-bridging hypothesis* of shimmering [7,9,12] predicts that surface bees are affected one-by-one *continuously* and *linearly* along a propagation line according to three principles: the first principle is that propagation is *directed*, whereby a surface bee is stimulated to participate in shimmering by her neighbour bees in those angular sectors where shimmering cohorts show maximal activity [9]. The second principle of *bucket bridging* is that shimmering activity proceeds steadily from one agent to the next in a *linear* fashion [7,9]. The third principle is that information is transmitted in parallel chains of agents (for a summary of abbreviations and definitions, see Glossary S1). Theoretically, if information generated at a certain spot propagates in parallel queues at exactly the same velocity, the frontline of the wave would represent a single row of shimmering bees. Any deviation from this parallel propagation will broaden the wave front. The directivity in propagation based on these three principles was addressed in the *directed-trigger* hypothesis of *bucket bridging* [9].

Although shimmering is a collective, synchronized and cascading behaviour, each agent is seemingly free to decide whether to participate in shimmering or not. Furthermore, agents that do participate flip their abdomens at variable strengths and angles of up to 120°. The starting point of shimmering depends on the position of the threatening cue [11–12], from where it spreads into all directions, similar to mechanical analogues of water or sound waves [16–17]. However, shimmering does have different ways to propagate [9,11–12]. Apart from *bucket-bridging* [7–9], shimmering

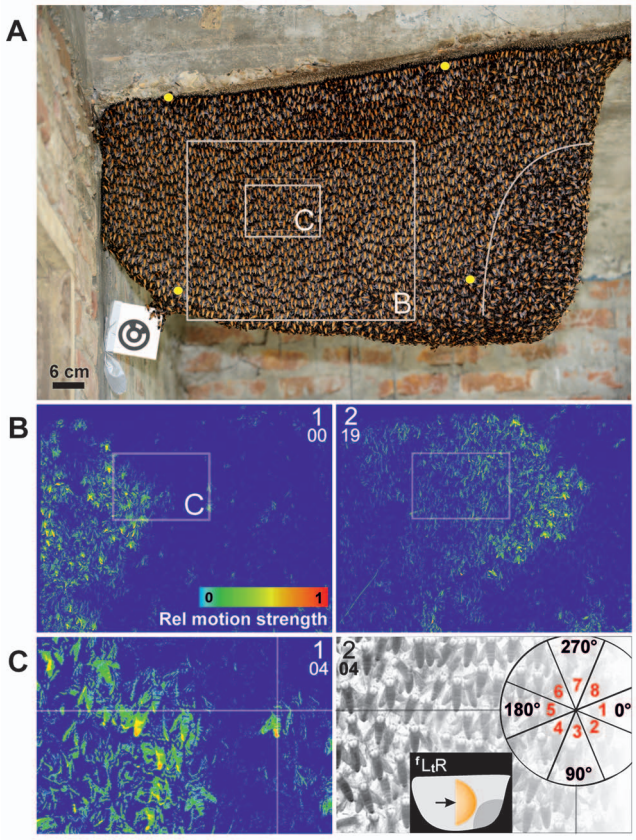

Figure 1. Experimental nest of Apis dorsata. (**A**) High resolution photo of *nest B*; grey open squares refer to the boundaries of the images of the panels B and C; the four yellow points mark the corners of the image part in Movies S1, S3 and S5. In the mouth zone the surface bees are randomly oriented (which is visible at the right side and below the white curve); peripheral to the mouth zone the surface bees are mostly vertically oriented, with their heads upwards and abdomens downwards. (B–C) Differential images (see image analysis in Methods, [7]) from high resolution video recordings (fps = 60 Hz) of nest part specified in the panel A (real-world measures of panels: B/43×34 cm; C/14×10 cm); large capital numbers show the panel count, small numbers give the relative count of frames during the propagation of the shimmering process which took place from left to right ($^{f}L_{t}R$) in the image. The rectangle in panel B indicates the boundaries of panel C. The time difference between the images of B_1 and B_2 was 317 ms [≡19 ff]. Pseudo colours (panels $B_{1,2}$ and C_1) visualize 8-bit Δ *lum* values of *motion strength* pixelwise in the rainbow palette with *blue* = 0, *red* = max Δ *lum* (see scale in B_1 and Methods). (C_2) The same image as in panel C_1 but in black-and-white and inverted for better discrimination of the abdomens; at the crossing points of the both marker lines an *agent bee* was selected which was moving solitarily ahead the shimmering front which was proceeding from the left to right; the schematic on the right gives the angular sectors of the *near neighbourhood* of this *focus bee* (with the directional categories; r_{Nh}<40 mm).
doi:10.1371/journal.pone.0086315.g001

waves appear to "jump" from specific sites to others [11–13], typically in increments of ten to fifteen surface bees, in a *saltatoric* process.

Here, we investigated the contribution of both, *bucket-bridging* [9] and *saltatoric* processes, to shimmering. The main characteristics of wave propagation were determined on the single bee level regarding recruitment, velocity and directionality, and three functional types of information transfer were distinguished. We found that the *saltatoric* process is associated with the generation of subordinate or *daughter* waves. By merging of *daughter* and *parental* waves, shimmering waves are speeded up by a factor of two to five, likely reinforcing the anti-predatory impact of shimmering [6].

Materials and Methods

Experimental conditions

Site and recording. The shimmering behaviour of giant honeybees was studied under field conditions during two expeditions to Nepal. The recording setup (see below) was established at three sites on the campus of the Tribhuvan University in Rampur (February 2009: nest A) and at the border of the Chitwan National park (February 2009: nest B [Fig. 1A]; November 2010: nest C). Two synchronized cameras were used to record black-and-white images with a resolution of 2,352×1,728 pixels (px), whereby one pixel covered approximately 0.30 mm in real-world coordinates. Therefore, the characteristic abdomen width of 6 mm of a giant honeybee was imaged by roughly 20 px. The cameras captured 60 frames per s (fps), resolving the abdomen-flipping phase of an individual bee of 200 ms within 12 frames (for further details see [6–9,12–13]). Nests were also filmed with a high-definition video camera (Panasonic HVX 200) at 50 fps and a resolution of 1,280×720 px from distances between 1.5–10 m, whereby the camera angle always covered the whole nest. Nest B was used for an automated in-depth analysis of the data recorded for approximately 11,000 focus bees and 460,000 neighbour bees (see below). The validity of the results from nest B was confirmed by manual analysis of selected aspects from other nests (see Results). This confirmation, together with our previous experience with many other nests [5–9,11–13] made us confident that the parameters used to describe shimmering behaviour previously and in this paper do not represent colony- or nest-specific traits, but can be considered as representative for the behaviour of *Apis dorsata* generally.

Dummy wasp stimulation of bees. For eliciting shimmering waves, colonies were stimulated with a dummy wasp fixed to a cable car device [7–9,13] at the sun-exposed side of the nests. A dummy with white, yellow and black stripes was made of Styrofoam (LxWxH: 40×15×15 mm) and suspended from a thin thread. Close to the mouth zone, the dummy was swung horizontally at an angle of 90° perpendicularly to the nest. The movement of the dummy was computer-controlled at variable velocities (0.1–0.5 m/s) and directions (towards and away from the nest). For more intense stimulation the dummy was connected to a 1.5 m long stick and moved manually (see Movie S1).

Characterization of shimmering

Identification of agents. In a giant honeybee nest, the colony members are arranged on both sides of the central comb in several layers, whereby several functional regions can be discerned, such as the *mouth* zone [10], the attachment zone, the rim zone and the *quiescent* zone [6–9,11–13]. Shimmering behaviour is mainly seen in surface bees in the *quiescent* zone ([7–9,12]; Movies S1, S2, S3, S4, S5, S6), flipping their abdomens upwards at an angle of up to 120°. In each frame, such agents were identified individually by stereoscopic imaging [7,9] using the coordinates of their thoraces, measured as x- (horizontal directions), y- (vertical directions) and z- (directions towards and away from the comb) positions at resolutions of fractions of a millimetre. More than 600 agents were continuously tracked in successive frames throughout multiple shimmering processes. A total of over 50 episodes of 2 min duration, each comprising 2 waves, were recorded and analysed under defined stimulation protocols [7,9].

Definition of spreading directions. The bee curtain of giant honeybee nests displays a polar topology where the individual bees are arranged with their heads upwards and their abdomens downwards ([7,9]; Fig. 1). Four key directions of wave spreading were defined ($dir_{WAV} \in \{1..4\}$), namely two horizontal directions (*from Left to Right* [$^{f}L_tR$] and *from Right to Left* [$^{f}R_tL$], whereby *Left* and *Right* refer to the recorded image), and two vertical directions (*from Top to Bottom* [$^{f}T_tB$] and *from Bottom to Top* [$^{f}B_tT$]).

Assessment of motion strength. The image-analysis software Image-pro plus (Media Cybernetics) was used to measure the parameter M_{xy} [7,9] that quantifies the motion of an individual agent bee. M_{xy} refers to the luminance changes ($\Delta lum = lum\ [f_i] - lum\ [f_{i-1}]$) in a 60×60 px zone around the thorax of the selected agent bee and was assessed in differential images (e.g. Fig. 1B,C_1; [6–9,12–13,15]) by pixel-wise subtractions of data from one frame (f_{i-1}) to the consecutive one (f_i) at intervals of $\Delta t_{ff} = \Delta t\ [f_{i-1}, f_i] = 16.67\text{ms}$ (fps = 60 Hz). The value M_{xy} includes mainly positional changes in horizontal (*x*-) and vertical (*y*-) directions, as well as movements of head, abdomen and extremities, such as legs, antennae or wings. Bees can move actively during *shimmering* [9–14], *flickering* [12–13] or locomotion (i.e., moving around on the nest surface or penetrating into or emerging from the subsurface layers of the nest). Bees can also be shifted passively when affected by the movements of their immediate neighbours [7]. Values for quiescent conditions were $M_{xy} = 0.3 \times 10^4 \text{px per } \Delta t_{ff}$, and for massive shimmering activity they were $M_{xy} = 1..10 \times 10^4 \text{px per } \Delta t_{ff}$. Values for M_{xy} were normalised as $^{rel}M_{xy}$ relative to the maxima in each recording [7,9], because they depend on conditions of video recording such as lighting and zoom mode used, and on image analysis tools such as subtraction, filtering and segmentation.

Determination of time zero. When the wave front arrived at an agent bee, weak deflections in $^{rel}M_{xy}$ values of the agent bee were assessed [7,9] even before she started to flip her abdomen (Fig. 2). Such small motions of an agent bee were caused by the shimmering-active neighbours. During abdominal flipping, the $^{rel}M_{xy}$ value sharply rises and peaks within 40 ms. In addition, the arrival of the wave can be traced by this parameter some frames before the abdominal flipping, which caused a slight increase in the $^{rel}M_{xy}$ value (for details, see Figs. 2,3A and [7]). This transient increase allowed identifying a *shimmering incident* defined as the flipping of the abdomen of an individual agent bee participating in the shimmering wave. A *shimmering incident* was only considered if the agent exceeded the threshold (th) value of $\Delta M_{th} = 10$ px for at least five successive frames in the differential images (Equation 1). This criterion served to supress noise.

$$\Delta M_{xy} = (M_{xy}\ [f_5] - M_{xy}\ [f_1]) > \Delta M_{th} \qquad (1)$$

For each *shimmering incident* (Figs. 2,3A) the following parameters were assessed: (a) the start time zero (t_0) was defined one frame before the sharp rise of $^{rel}M_{xy}$ detected by the trigger algorithm at the time t_{th} when the motion strength exceeded the threshold value according to $t_{th} = t\ [f_{th}]$ and $t_0 = t\ [f_{th} - 1]$.

(b) The motion strength of the *shimmering incident* of a selected agent was defined by the maximal $^{rel}M_{xy}$ value measured within 10 frames after t_0. These strength values were graded in eight steps proportional to the $^{rel}M_{xy}$ values (with motion strength categories $c_{Mxy} \in \{1..8\}$). Hereby, the assignment of $c_{Mxy} = 1$ was particularly important, as this minimum level of active shimmering motion of a selected agent bee had to be clearly distinguished from unambiguous (passive) sub-threshold motions (cf. Fig. $2A_2$). Only active, supra-threshold movements with $c_{Mxy} \geq 1$ were considered. In contrast to the agent-related $^{rel}M_{xy}$ values the pseudo colours of differential images (Figs. 1–2,4–5) visualize the relative motion

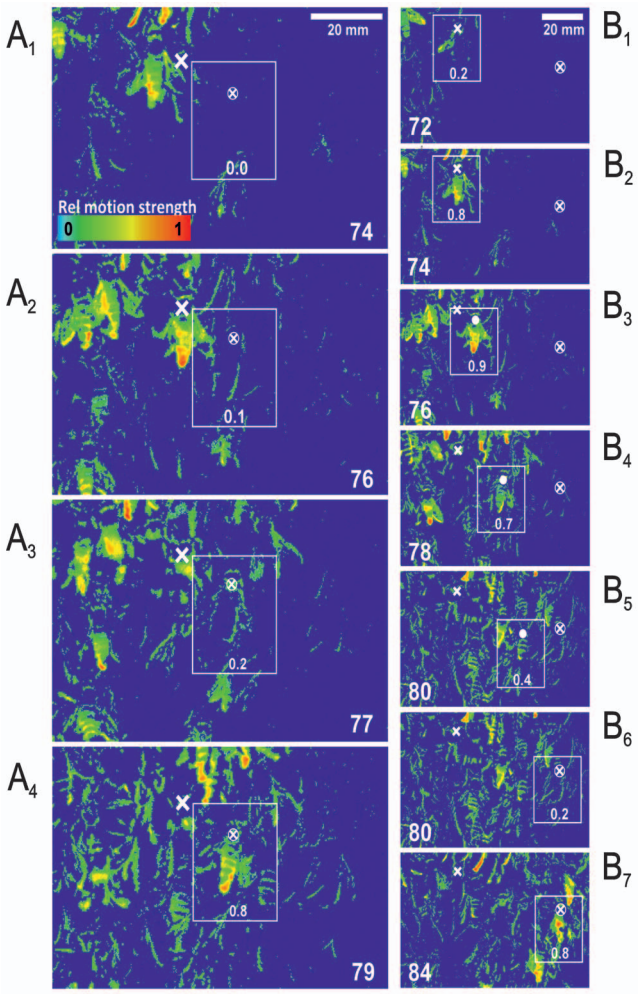

Figure 2. Two examples of bucket-bridging in the signal propagation of shimmering of A. dorsata. (A_{1-4}) Information transfer from left to right ($^{f}L_tR$) in the images, displayed over six frames (from f 74 to f 79≡100 ms) from the *focus bee* (whose thoracic position was marked with a white cross throughout the frames) to one of her neighbours (whose thoracic position was marked with a white cross in a white circle); differential images represent luminance [Δ *lum*] patterns according to the rainbow scale displayed in panel A_1 (see Fig. 1 and Methods), the grey open rectangles signify the extension of the receiver agent, the numbers at the bottom of the rectangles refer to the relative activation level of the *shimmering incident* (whereby the pixel-by-pixel luminance differences were scaled on the rainbow palette with $^{rel}M_{xy} = 0.0..1.0$; for the estimation of the momentary expression of motion strength, see Equations 2a,b for retrograde and prograde extrapolation in Methods under "Benchmarking *bucket-bridging*"). (B_{1-7}) Information transfer from a *focus bee* (thoracic position marked with a white cross) over a chain of four neighbours to a target agent; the thoracic positions of intermediate neighbours were marked by closed white circles, that of the target agent with a white cross inserted in a white circle; this target bee was passively moved from B_4–B_6, and flipped her abdomen in B_7); the white open rectangles signify the range of the respective agent along the selected chain, the numbers inside the rectangles give the respective activation levels.
doi:10.1371/journal.pone.0086315.g002

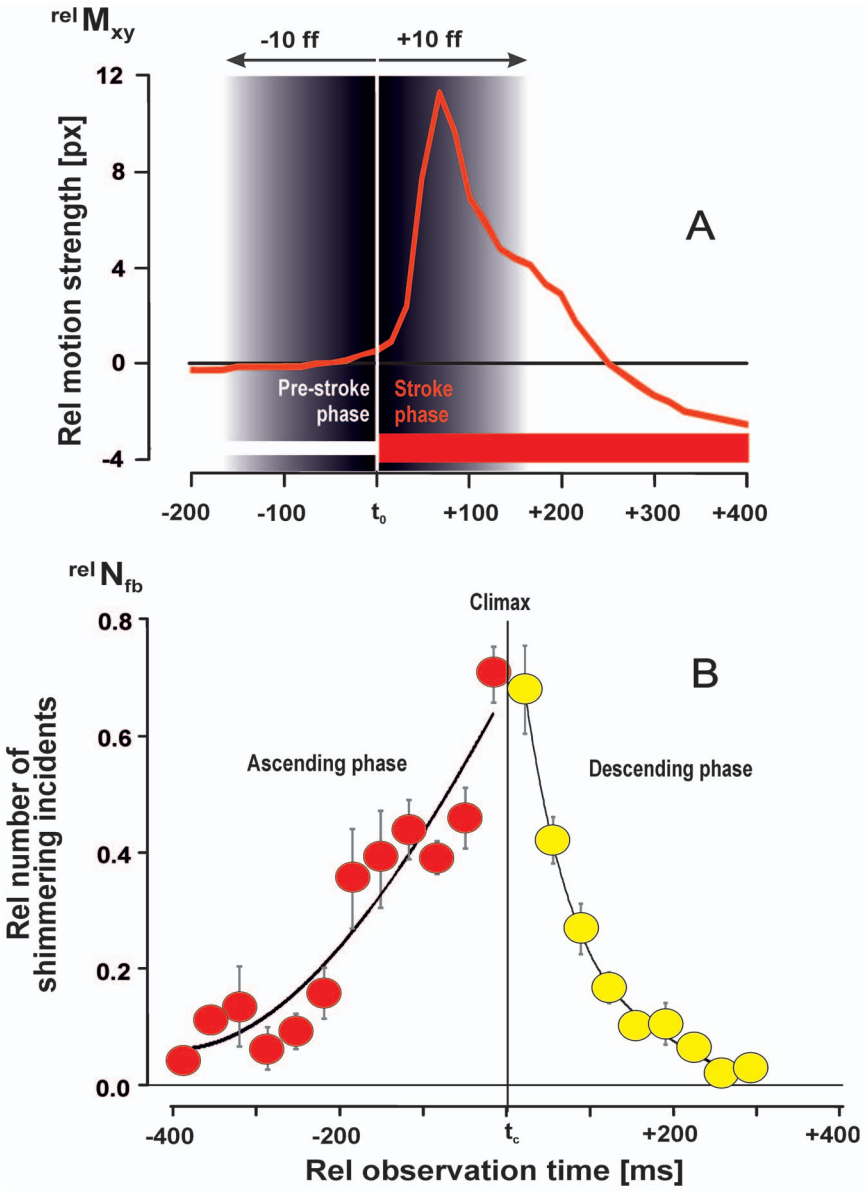

Figure 3. Definition of a shimmering incident and of the three phases of a shimmering wave. (A) Typical time course of the motion of an individual *focus bee* during abdominal flipping (termed *shimmering incident*): ordinate: relative motion strength assessed by ${}^{rel}M_{xy}$ (for definitions, see Methods). Abscissa, observation time in ms; t_0, start time of the *shimmering incident* of the agent, and start time of the *stroke* phase, synonymous to the *post-*$[t_0]$*-stroke* phase; Grey shaded zone, the time window of $\pm$167 ms ($\equiv t_0 \pm$10 ff) for categorizing the communication *status* of agents (see text). (B) The three phases (*ascending*, *climax*, *descending*) of a shimmering wave can be categorized by the course of recruitment of agents participating in a wave, quantified by the relative number of *shimmering incidents* which were traced per image at the relative observation time ${}^{rel}t$ with ${}^{rel}N_{fb}\,[{}^{rel}t] = N_{fb}\,[{}^{rel}t]\,/_{\max}\Delta\,N_{fb}$ [per wave] and $N_{fb} = 10{,}894$ (see Methods; n = 25 episodes of 2 min duration). Full circles, arithmetical, vertical bars, SEMs; n = 40 waves. The time t_c gives the time point of the *climax* when the maximum number of *shimmering incidents* ($_{\max}N_{fb}$) occurred simultaneously. Red colour marks the *ascending* phase (${}^{rel}t < t_c$) of the shimmering waves, yellow colour marks the *descending* phase (${}^{rel}t > t_c$).
doi:10.1371/journal.pone.0086315.g003

strength by the luminance differences pixel by pixel, scaled with ${}^{rel}M_{xy} = 0.0..1.0$ on the rainbow palette.

Focus bees and their neighbours. The participation in shimmering greatly varies from agent to agent and ranges from passive motions (Fig. $2A_2$) caused by the approaching wave front to active participation with abdominal flipping at variable strengths (Fig. 3A). To support the automated evaluation and sorting of the various types of *shimmering incidents*, the concept of the *focus bee* was introduced. For every *focus bee*, two sets of *neighbour bees* (nb) were defined, which were positioned in the *near neighbourhood* (<40 mm; Fig. $1C_2$) and in the *far neighbourhood* (>40 mm, <100 mm). The numbers were distinguished according to whether these neighbour agents had participated in shimmering before (N_{nb}^{pre}) the wave front arrived at the *focus bee*, or afterwards (N_{nb}^{post}). Thus, an agent bee was treated either as a *focus bee*, or as a *neighbour* bee.

In the in-depth study, *focus-bee* or *neighbour-bee* status was assigned to agents regarding all four main wave directions ($dir_{WAV} = {}^{f}R_t L$: $N_{fb} = 2{,}823$; $N_{nb} = 138{,}190$ [for >40 mm, <100 mm]/29,248

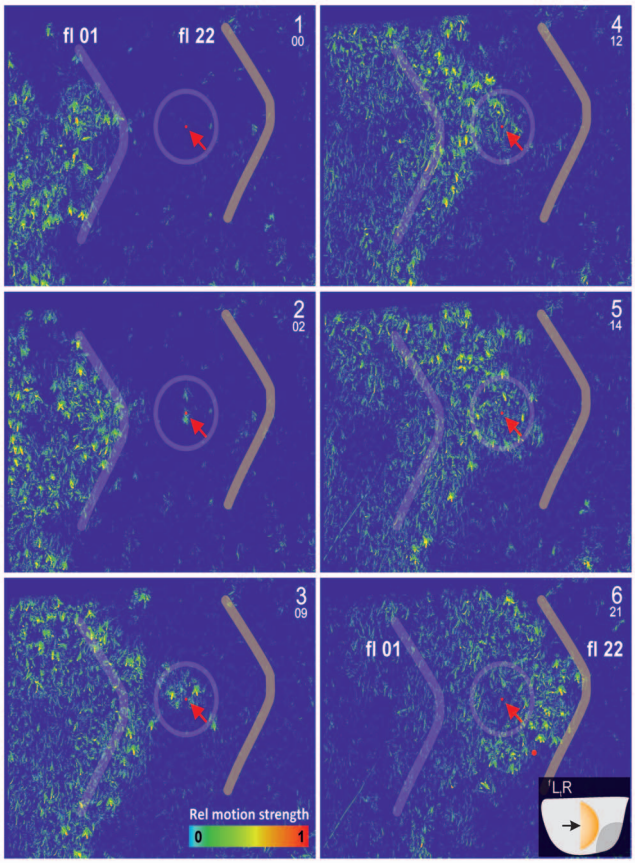

Figure 4. Propagation of a shimmering wave across the nest surface (survey view). This example refers to a wave that spread from left to right ($dir_{WAV} = {}^{f}L_tR$) in the image. Capital letters in the right corners (1–6) show the panel count, small numbers give the relative count of selected frames (ff 01–22), comparable to Figs. 1, 2 and 4 (for distance measures, see Fig. 1B). The pseudo colour bar in panel 3 shows the scale for the relative motion strength (see Fig. 2). For better comparison, the thick grey line fl 01 gives the *front line* of the (*parental*) wave manually drawn in panel 1 (at f 01), and the line fl 22 shows the front line of the same wave 384 ms later (at ff 22); red points marked with red arrows show the thorax of the *focus bee* selected in this wave, which flipped her abdomen at f 02 and generated a *daughter* wave that subsequently merged with the *parental* wave at f 12. The circles around the *focus bee* indicate the range of the *near neighbourhood* (<40 mm).
doi:10.1371/journal.pone.0086315.g004

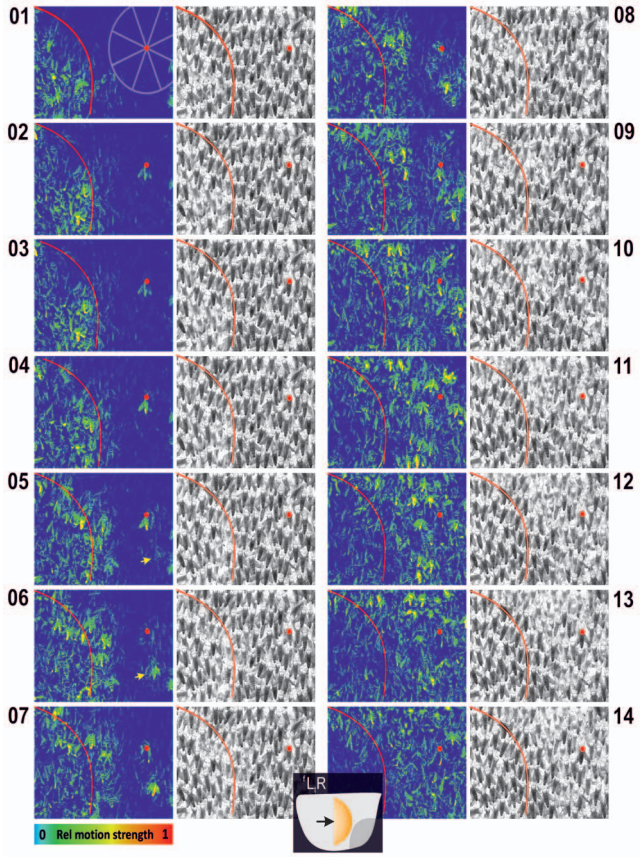

Figure 5. Propagation of a shimmering wave across the nest surface (detail view). The same wave is shown as in Fig. 3 but zoomed (for distance measures, see Fig. 1C). Continuous sequence of frames as pseudo coloured differential images and inverted video images; numbers (01–14) indicate the relative frame counts (fps = 60 Hz with interframe intervals of 16.67 ms). Scale below panel f 07 shows the relative motion strength (see Fig. 2). Red dots indicate the selected *focus bee* (the same as in Fig. 4) that started to flip her abdomen at f 02, acting as a *generator bee* for the subsequent *daughter* wave. One of her neighbours (marked with a yellow arrow) was passively shifted in f 05 and started the abdominal flip in f 06. The resulting *daughter* wave merged with the *parental* wave at f 10. The red curves on the left side of the images are shown for comparison with the initial position of the *parental* wave front as indicated in f 01.
doi:10.1371/journal.pone.0086315.g005

[for <40 mm]; ${}^{f}L_tR$: $N_{fb} = 3{,}098$; $N_{nb} = 159{,}417/44{,}939$; ${}^{f}B_tT$: $N_{fb} = 3{,}396$; $N_{nb} = 105{,}356/13{,}211$; ${}^{f}T_tB$: $N_{fb} = 1{,}577$; $N_{nb} = 56{,}595/9{,}539$; all wave directions: $N_{fb} = 10{,}894$; $N_{nb} = 459{,}558/96{,}937$, where fb and nb stand for *focus bee* and *neighbour bee*, respectively). For most results shown in this paper, waves in the direction $dir_{WAV} = {}^{f}R_tL$ were taken as representative of all four data sets.

Trigger neighbours. The time point t_0^{fb} of a *shimmering incident* of a *focus bee* was used to define the potential *trigger neighbour bee* for a given *shimmering incident* (Fig. 3) by considering two criteria: First, the *trigger neighbour* must have already participated in the same wave before the *focus bee*; however, this participation was only considered if this neighbour was active within the time window of 88 ms (−5 ff) prior to t_0^{fb}. Second, the agent defined as *trigger neighbour* had to be positioned closest of all other candidates to the *focus bee* and in her *near neighbourhood*. This criterion excluded those bees from analysis that flipped their abdomen outside the *near neighbourhood* (in many cases such bees generated *daughter* waves; Figs. 1–2, 4–5). The *trigger direction* of a *focus bee* (α_{TRIG}^{fb}) was defined by the angle of the direction of her trigger neighbour, measured from the position of the *focus bee*, categorized according to the eight sectors of neighbourhood ($dir_{Nh} \in \{1..8\}$; Fig. $1C_2$) in which the trigger neighbour was positioned.

Relative time scales of focus bees and their neighbours. The time courses of the *shimmering incidents* of selected neighbour bees were synchronized to the time t_0^{fb}. This synchronization conjoined the movements of *focus bees* and her triggering neighbours with the positional (x,y,z) parameters and the ${}^{rel}M_{xy}$ values. This enabled sorting and pooling of identified *focus bees* and their neighbours, collected at different locations and times according to *main wave directions* ($dir_{WAV} \in \{1..4\}$), *motion strengths* ($c_{Mxy} \in \{1..8\}$), and *trigger directions* ($dir_{TRIG} \in \{1..8\}$) for further statistical analysis.

Benchmarking of bucket-bridging. *Bucket bridging* was characterised for manually selected agents by the assessment of the information transfer between two neighbouring bees (Fig. 2A), and over a chain of adjacent agents (Fig. 2B). The thorax-to-thorax distances were calculated in mm. A motion detection method was used that utilized differential images (see above) considering the following criteria [9]: (a) Chains of agent pairs were selected (Fig. 2), in which *emitter bees* (which flipped their abdomen first) could clearly be distinguished from *receiver bees* (which followed the action of the *emitter* bee) throughout a continuous and linear sequence of actions. (b) *Emitters* and *receivers* participated in the same *chain* (see Introduction and [9]). (c) Bees were excluded from data assessment if they did not show any interaction, if they were activated synchronously (instead of sequentially, i.e. they did not participate in the same chain) and if they showed abdominal flipping with a delay larger than 167 ms (≡10 ff). (d) In differential images, the temporal information transfer was estimated using the abdominal flipping of the *emitter* and the *receiver* bee. The time t_0 was determined by weighting M_{xy} values in deciles whereby ${}^{rel}M_{xy}=0.0$ indicated *quiescence* of the *focus bee* ($\Delta lum<8$), and ${}^{rel}M_{xy}=1.0$ defined a fully lifted abdomen. The first and last frames (f_1,f_{last}) with traces of motions of individual agents were weighted accordingly (${}^{rel}M_{xy}\,[f_1]$, ${}^{rel}M_{xy}\,[f_{last}]$) to estimate the start and end points of information transfer (t_{start}, t_{end}) by bucket bridging. This measure retraced the start point of abdominal flipping by retrograde extrapolation (Equation 2a) on the basis of the weighting value ${}^{rel}M_{xy}\,[f_1]$. Similarly, the abdominal flipping of the last bee in a chain was calculated by determining the last frame (f_{last}) with motion activity by prograde extrapolation (Equation 2b).

$$t_{start}=t\ [f_1]-(\Delta t_{ff}\times {}^{rel}M_{xy}\ [f_1]) \tag{2a}$$

$$t_{end}=t\ [f_{last}]+(1-{}^{rel}M_{xy}\ [f_{last}]\times\Delta t_{ff}) \tag{2b}$$

Ethics Statement

The research expedition to Chitwan, Nepal, entitled "Study on the behaviour of the giant honeybees: Observations and recording of behaviours at the nesting site" was supported by the Rector of the Centre for International Relations of the Tribhuvan University (Kathmandu, Nepal).

Results

Bucket-bridging

An example of *bucket bridging* is shown in differential images in Fig. 2A$_{1–4}$ (ff 74–79 corresponding to 100 ms). The *emitter bee* showed maximum activity in f 76. The silhouette of the *receiver bee* was already visible in f 76, when it was slightly moved passively by the advancing wave front. In f 77, the shape of the right forewing of the *receiver bee* appeared, indicating active participation in shimmering. In f 79 her abdomen started to be lifted actively, followed by a massive motion of the whole body accompanied by a beat of both wings.

An individual abdominal flipping typically lasts 67.16±0.97 ms (mean ± SE; n = 174 abdominal flips; Figs. 2, 3A, 4; [14]). The manually evaluated shimmering waves (n = 47) showed that information transfer between adjacent shimmering-active neighbours (positioned at distances of d_{bb} 15.94±0.66 mm, where bb stands for *bucket bridging*) was completed within $\Delta t_{bb}=39.16\pm2.84$ ms (Fig. 2A$_{1–4}$), corresponding to a velocity of $v_{bb}=0.5085\pm0.0413$ m/s. However, with $v_{bb}=0.317\pm0.0145$ m/s the speed was lower when assessed over a short chain of agents (Fig. 2B, $n_{bb}=2.60\pm0.17$ bees; $d_{bb}=43.32\pm1.98$ mm; $\Delta t_{bb}=107.90\pm8.58$ ms; n = 40 shimmering waves). We then used this speed value ($v_{bb}=0.317$ for nest B) as a benchmark for characterizing the *bucket-bridging* process. For comparison, similar speed values were found for nests A and C (nest A: $v_{bb}=0.2461\pm0.0193$ m/s, n = 28 shimmering waves; nest C: $v_{bb}=0.3598\pm0.0263$ m/s, n = 26).

Saltatoric processes

Saltatoric wave propagation involves bees that are more than 80 mm away from the approaching wave front, and lift their abdomens typically 30–50 ms earlier than other participants in their own *near neighbourhood*. These bees generate *daughter* waves and are termed *generator* agents. In Figs. 4,5 (compare Movies S1, S2, S3, S4, S5, S6), one of these *generator* agents is marked by a red point on the thorax. During the abdominal lifting of this agent (ff 02–06, Fig. 5), the *parental* wave (pw) moved from left to right in the image. Using the position of the wave front in two subsequent frames the velocity of the *parental* wave was found to be $v_{pw}=0.239$ m/s, which is in the same order of magnitude as calculated for *bucket bridging* in the same nest (Fig. 2A).

In f 09 of Fig. 4 the *daughter* wave is visible as a small circular batch, and in f 12 this *daughter* wave started to merge with the *parental* wave. The frontline of the *parental* wave "jumped" from the left to the right side of the *daughter* wave (from f 10, immediately before the *daughter* wave merged with the *parental* wave, to f 11, just after merging) within 16.67 ms or even less. The frontline of the merged waves advanced over a distance of 160 mm, which corresponds to an acceleration of the shimmering velocity (v_{sh}) to a value of at least 0.960 m/s by *saltatoric* information transfer. This is roughly three times faster than *bucket-bridging* alone.

Fig. 5 demonstrates the *saltatoric* information transfer in more detail for the same *focus bee*. This bee started abdominal flipping in f 02, and one of her neighbours joined 70 ms later (marked by a yellow arrow, first visible in ff 04–05). Subsequently, other neighbours followed, producing a *daughter* wave. The *parental* wave on the left side of the image continued to spread to the right, while the daughter wave spread into all directions by *bucket bridging*. Finally, 170 ms after the start of abdominal flipping of the *generator* bee (in f 10), the *daughter* wave merged on its left side with the *parental* wave, while the frontline of the merged waves "jumped" to the right side of the former *daughter* wave.

Propagation velocity of shimmering waves

A shimmering wave lasts up to 800 ms (Fig. 3B) and includes the *ascending* phase of 200–300 ms, in which the number of synchronously shimmering surface bees increases to the maximum, the *climax* phase, when a maximum number of agents were simultaneously active (lasting approximately 200 ms), and the *descending* phase (300–400 ms), in which the number of synchronously shimmering surface bees decreases ([6,12] and Fig. 3B). When measured from the start to the end of a wave by the detection of the positions of the wave fronts in differential images (Figs. 1–2,4–5), v_{sh} was calculated to be 0.367 ± 0.020 m/s (n = 10 waves, see Movies S1, S2, S3), similarly slow as found for *bucket bridging*.

Alternatively, when measured during the *climax* phase, v_{sh} was 0.514 ± 0.019 m/s, significantly ($P<0.01$, Student's test) faster than the benchmark value for *bucket bridging* ($v_{bb}=0.325$ m/s). The v_{sh} value for the *climax* phase was calculated for the wave direction $dir_{WAV}={}^{f}R_{l}L$ regarding nest B by selecting pairs of agents that

were positioned horizontally (at an angle of $\alpha_{WAV} = 7.95 \pm 5.40°$; n = 41 waves; definition of angle of wave direction in Fig. $1C_2$) at a distance of 112.90±4.08 mm between those *emitters* and *receivers* that were subsequently affected by the same wave fronts within ten frames or more (226.06±8.21 ms) in a straight line (cf. Fig. 2B).

This v_{sh} value of 0.514±0.019 was taken as a benchmark value for the mixed propagation mode (*bucket bridging* and *saltatoric* processing). Hence, v_{sh} during the *climax* phase is faster than during the start or the end phases, likely due to the higher probability of the occurrence of *saltatoric* events.

Communication statuses of agents

The contributions of individual agents to the spreading of shimmering waves, i.e. to *bucket bridging* or *saltatoric* propagation were assessed by automated techniques using the algorithms described below. The "communication status" of a *focus bee* was characterized spatially and temporally by considering her *neighbours* in the *near neighbourhood* as a reference region (<40 mm, see schematic in Fig. 6), and the *pre-stroke* and *post-stroke* intervals of ±167 ms (≡±10 ff) as a reference time window, whereby the abdomen flipping commenced at the time t_0. Shimmering waves were assessed regarding four wave directions (Table S1, [7]), and for in-depth analysis of communication status the wave direction

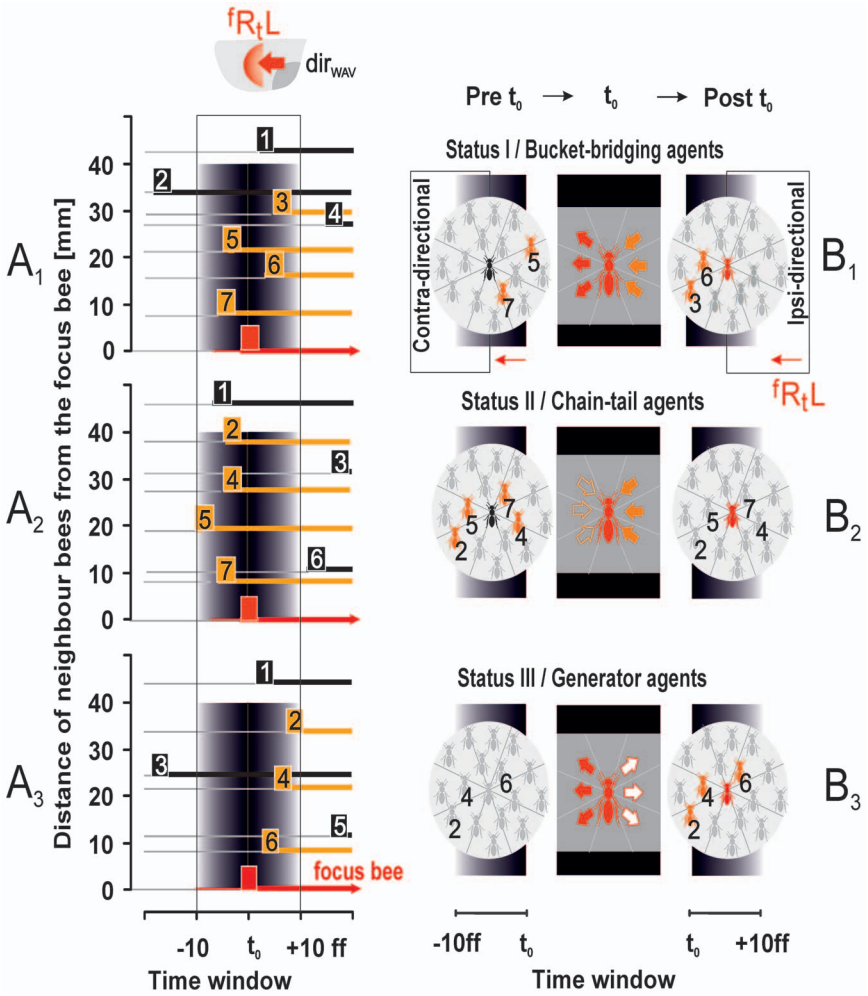

Figure 6. Definition of three communication statuses of surface bees (shown for the wave direction $dir_{WAV} = {}^{f}R_tL$). Sketches of activity plots for distinguishing the *statuses* (*I,II,III*) of *focus bees*. (A_{1-3}) *Focus bees* are marked by red full rectangles at t_0; abscissa, time in frames (fps = 60 Hz) in relation to $[f^{\lceil}[t_0]]$ when the *focus bee* started her flipping; ordinate, distance of neighbours from the *focus bee* in mm; grey thin horizontal lines symbolize the *quiescent* state of the sample agents; small full rectangles with numbers mark the onset of their abdominal flips; orange coding refers to positions of the neighbours within the *near neighbourhood* (<40 mm) with flipping activities within the critical time window of ±10 ff; black coding refers to complimentary attributes (>40 mm; >|±10 ff|). Thick horizontal lines (black, orange, red) symbolize that abdomen flipping is still going on. (B_{1-3}) The panels *Pre* t_0 and *Post* t_0 display the *near neighbourhood* of a *focus bee* which is marked black when quiescent and marked red when she flips her abdomen. The numbers and colour codes of shimmering-active neighbours are the same as in the panels A_{1-3}; arrows of the central panels (regarding the time t_0) explain the directions of information transfer: *status I* (*bucket-bridging*) agents in the *pre-stroke* (*Pre* t_0) phase receive mechanical information (full orange arrows) predominantly from the side from where the wave came, in the *post-*$[t_0]$*-stroke* (*Post* t_0) phase information is transmitted predominantly to the side where the wave is spreading to (open red arrows); *status II* (*chain-tail*) agents receive and emit mechanical information but fail to recruit other neighbours as transmitters; *status III* (*generator*) agents utilize predominantly visual information from the threatening cues, but not from shimmering-active agents in their *near neighbourhood*. They are leaders in emitting mechanical information and generate *parental* or *daughter* waves.
doi:10.1371/journal.pone.0086315.g006

$^{f}R_tL$ (N_{fb} = 4,025; N_{nb} = 29,248 [for <40 mm]) was selected as representative for all waves.

Three communication *statuses* (*I–III*) of *focus bees* were distinguished. *Status I agents* are driven by shimmering-active neighbours in the *pre-stroke* phase, positioned at their *ipsi-directional* side (from where the wave came), passing information on to their *contra-directional* side (to where the wave is continuing) in the *post-stroke* phase (Fig. 6A_1,B_1). This strategy of propagating information conforms to *bucket-bridging* [7,9], and these bees are termed *bucket-bridging* agents. They comprised the majority of surface bees and were represented by 54.33% of agents at a reference window of ±2 ff (whereby "−2 ff" defines the time window in the *pre-stroke* phase and "+2 ff" the time window in the *post-stroke* phase). The number of *bucket-bridging* agents increased (Fig. 7A_{1-2},B_1) with the reference time window (±10 ff) up to a value of 74.98±2.83%. This increase was due to the definition of *status II* agents (Fig. 6A_2,B_2: see below), which may turn into *bucket-bridging* agents with increasing length of the reference window (Fig. 7). The neighbours of the *bucket-bridging* agents were similarly large in number in the *pre-stroke* and *post-stroke* phases (Fig. 7C_1, Table S2: N_{nb}^{pre} [at −10 ff] = 7.56±0.90; Fig. 7C_2: N_{nb}^{post} [at +10 ff] = 6.06±1.16) corresponding to 47.16% of all shimmering-active neighbours evaluated in the *pre-stroke* phase and to 41.01% of neighbours in the *post-stroke* phase.

In Fig. 8A, these *bucket-bridging* agents were sorted into two classes based on the number of shimmering-active neighbours in the *pre-stroke* and *post-stroke* phases (*class* $1: fb\,[N_{nb}^{pre} < N_{nb}^{post}]$); *class* $2: fb\,[N_{nb}^{pre} > N_{nb}^{post}]$). Hereby, the maximal numbers of neighbours found for *focus bees* were similar for both phases ($_{\max}N_{nb}^{pre} = 24$; $_{\max}N_{nb}^{post} = 26$) and both classes showed similar percentages (class 1: 50.27%; class 2: 49.73%; P = 0.1925, χ^2 test) with a polynomial distribution, when sorted in steps of 0.1 parts of the ratio $Q_{nb} = N_{nb}^{pre}/N_{nb}^{post}$; Table S1). This data symmetry applies to all phases of a shimmering wave (*ascending*, *climax* or *descending* phase; Fig. 3B and [6]). Furthermore, the selected wave direction $dir_{WAV} = {}^{f}R_tL$ (red symbols in Fig. 8) was found to be representative of all four wave directions investigated (black symbols in Fig. 8), which shows that shimmering is invariant regarding the direction of wave propagation (cf. [9]).

S*tatus II agents* flip their abdomens triggered by their shimmering neighbours, (Fig. 6A_2,B_2), but thereafter their *near neighbourhood* becomes quiescent. These bees terminate the information transfer in their chains and are, henceforth termed *chain-tail* agents. The relative numbers of *chain-tail* agents increased from $^{rel}N_{fb}$ = 9.20±0.94% (at −10 ff, corresponding to 166.67 ms, where ^{rel}N stands for relative number in per cent) to $^{rel}N_{fb}$ = 28.46±3.14% (at −2 ff≡33.33 ms; Fig. 7B_2) and had N_{nb} = 7.28±0.57 shimmering-active neighbours at −10 ff (Fig. 7C_3, Table S1).

In contrast to *chain-tail* agents, *Status III agents* (Fig. 6A_3,B_3) are not triggered by their neighbours [<40 mm] in a reference time window in the *pre-stroke* phase of −10 ff, but flip their abdomens before their neighbours do so. They generate *parental* or *daughter* waves (as demonstrated in Figs. 1,4–5 and Movies S1, S2, S3, S4, S5, S6) and are termed *generator* agents. In contrast to *status-I* and -*II* agents, *generator* agents occurred at numbers which were roughly independent of the length of the *post-stroke* phase (at +3 ff≡50 ms: $^{rel}N_{fb}$ = 17.65±2.69%; at +10 ff: $^{rel}N_{fb}$ = 15.82±2.61%; Fig. 7B_3, Table S1) and activated N_{nb} = 6.36±0.45 neighbours at +10 ff (Fig. 7C_4; Table S1), which corresponds to $^{rel}N_{fb}$ = 6.75% of the shimmering-active neighbours of all surface bees.

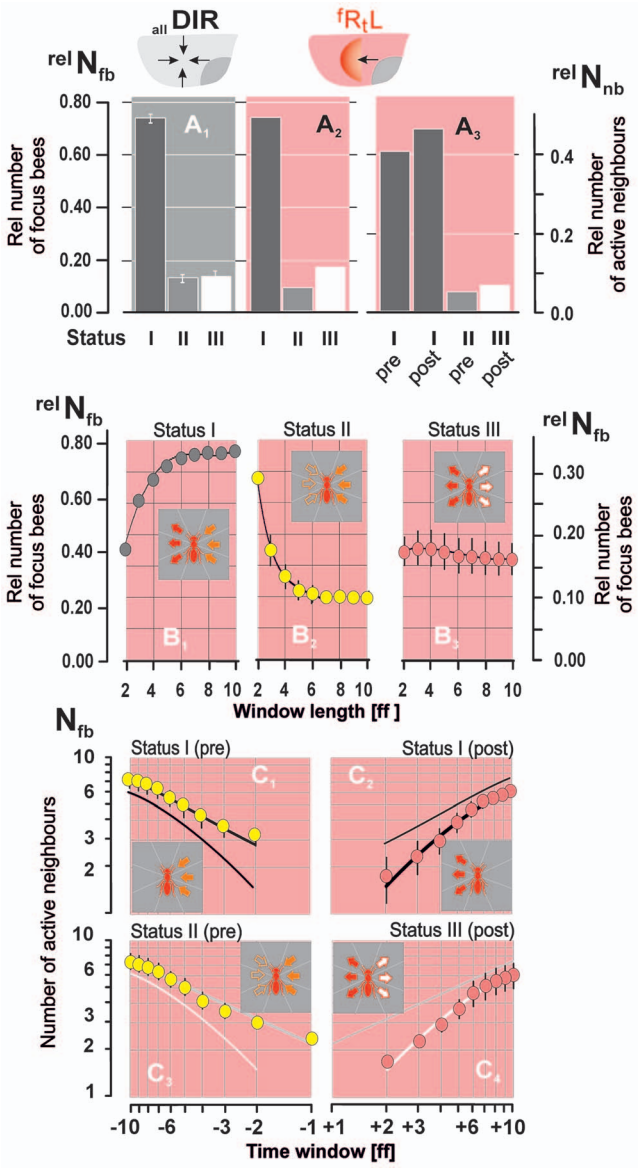

Figure 7. Properties of status I–III agents. (A_{1-3}) Rates of *status I–III* agents ($^{rel}N_{fb}$) regarding the four directions of wave propagation $dir_{all\ WAV}$ (grey background, panel A_1, N_{fb} = 13,678) and regarding the wave direction $^{f}R_tL$ (pink background, panel A_2, N_{fb} = 4,025); panel A_3, rates of shimmering-active neighbours ($^{rel}N_{nb}$) of *status I–III* agents ($^{f}R_tL$, N_{nb} = 29,248) in the respective *pre-stroke* (pre) and *post-stroke* (post) phases; see also Table S1. (B_{1-3}) Rates of *status I–III* agents ($^{rel}N_{fb}$) in dependence of the length of the discrimination window (abscissa in [ff], fps = 60 Hz). (C_{1-4}) Numbers of shimmering-active neighbours (N_{nb}) of *status I–III* agents depending on the length of the discrimination window (abscissa scaled as t_0±ff); ff<0 refers to *pre-stroke* phase (yellow coding), ff>0 to *post-*[t_0]*-stroke* phase (red coding). Columns (A) and full circles (B–C), arithmetical means; vertical bars, SEMs.
doi:10.1371/journal.pone.0086315.g007

In Fig. 8B,C *chain-tail* and *generator* agents were sorted according to the number of shimmering-active neighbours in the *pre-stroke* (−10 ff) and *post-stroke* (+10 ff) phases. These data distributions allow discerning agents with less than five shimmering-active neighbours (subgroup 1), and those agents with more than five active neighbours (subgroup 2). In both agent types, subgroup 1 was larger, while subgroup 2 converged to zero with increasing

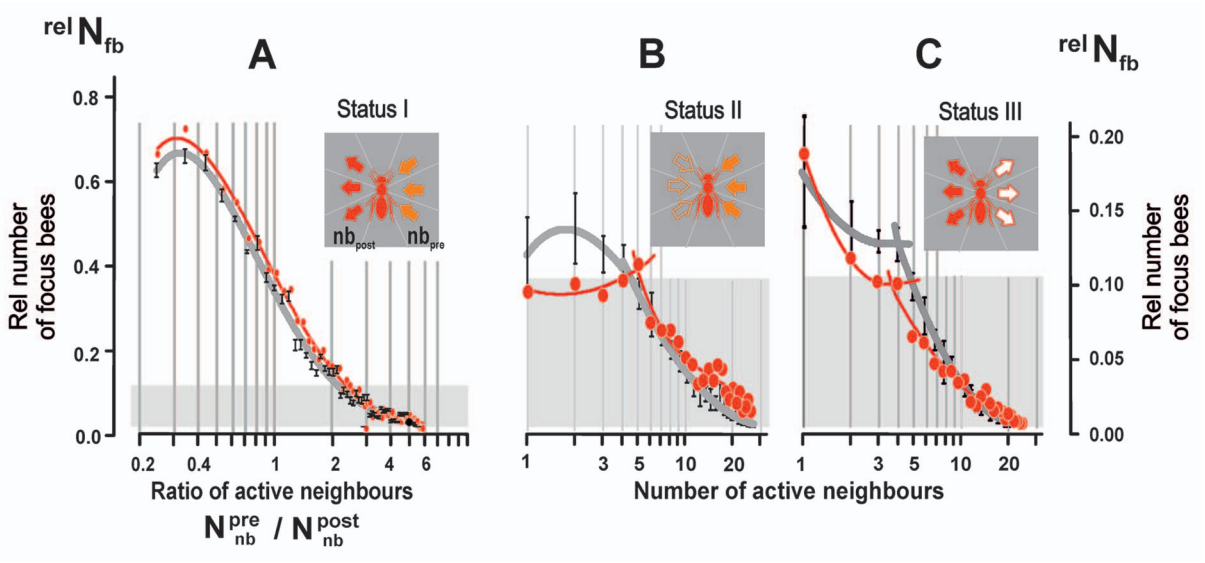

Figure 8. Relationship between status I–III agents and their neighbours. (A) The number of *status I* agents in dependence of the ratio of their shimmering–active neighbours in the *pre-stroke* and *post-stroke* phase ($Q_{nb} = N_{nb}^{pre}/N_{nb}^{post}$); abscissa, 57 classes of Q_{nb} in steps of 0.1; ordinate, rate of *focus bees* whereby the value ${}^{rel}N_{fb} = 1.0$ refers to the maximum number of cases per data set; red symbols: $dir_{WAV} = {}^{f}R_tL$ (n = 7 data sets); black symbols: $dir_{WAV} = dir_{all\ WAV}$ (n = 25 data sets); for regressions, see Table S1. (B,C) The rate of *focus bees* (${}^{rel}N_{fb}$) of *status II* & *III* in dependence of the numbers of their shimmering-active neighbours (N_{nb}); regressions of the mean values are shown into two parts: panel B: $N_{nb}<5$; $N_{nb}>5$; panel C: $dir_{all\ WAV}$: $N_{nb}<6$, $N_{nb}>5$; ${}^{f}R_tL$: $N_{nb}<5$, $N_{nb}>4$); for regressions, see Table S1. Full circles and mid positions of vertical bars, arithmetical means; vertical bars, SEMs.
doi:10.1371/journal.pone.0086315.g008

numbers of active neighbours (Table S1). Hence, only few shimmering-active neighbours (<5) suffice to trigger both agent types.

Acceleration of shimmering by saltatoric propagation

The propagation of shimmering is based on complex synchronous and cascaded recruitment of surface bees, and was simplified in a mathematical model (see lookup tables in Fig. 9) that considers both the *bucket bridging* and the *saltatoric* propagation mode under climax conditions. This model allows to assess the impact of both processes on the v_{sh} of the compound wave considering three parameters (where bb stands for *bucket bridging* and sp for the *saltatoric* propagation): (a) v_{bb}, this is the v_{sh} under solely *bucket-bridging* conditions (Fig. 9A), where v_{bb} was varied in the model from 0.10 to 0.45 m/s (the benchmark value is 0.317 m/s, see above); (b) v_{sp}, this is the v_{sh} characterised by the *saltatoric* propagation, which was set to $v_{sp} = 0.800$ m/s (Fig. 9A–C); this velocity was slightly below the value of $v_{sp} = 0.960$ m/s that was found for a single *saltatoric* jolt of the wave front in the example in Fig. 4 (note that v_{sp} is only of theoretical relevance because a real shimmering wave never spreads saltatorically alone and that *bucket bridging* is the dominant propagation mode of shimmering); (c) the *distance* d_{E-R} between the emitters and the receivers (E−R) in a chain of *bucket-bridging* agents; according to the conditions in the nest d_{E-R} was varied from 20 to 45 mm (Fig. 9C,D). These three parameters were used to describe two wave properties that result from the combination of *bucket-bridging* and *saltatoric* propagation: First, the factor k_{sp} (Equations 3a,b) by which shimmering is speeded up by the saltatoric process (Fig. 9A,B).

$$v_{sh} = v_{bb} \times k_{bb} + v_{sp} \times k_{sp} \quad (3a)$$

$$k_{sp} = (v_{sh} - (v_{bb} \times k_{bb}))/v_{sp} \quad (3b)$$

with the weighting factors in %: $k_{sp} = 1..100$ and $k_{bb} = 100 - k_{sp}$.

For the above benchmark values under climax conditions ($v_{sh} = 0.514$ m/s; $v_{bb} = 0.317$ m/s) the impact of the saltatoric component ($v_{sp} = 0.800$ m/s) was $k_{sp} = 41.5\%$ for v_{sh} (Equation 3b) and the complementary 58.5% for k_{bb} (Fig. 9B). Second, I_{dec} was considered, the time interval within which an agent "decides" whether or not to participate in shimmering (Fig. 9C; conforming with $I_{dec} = d_{E-R}/v_{sh}$).

The values of I_{dec} calculated for the distance of $d_{E-R} = 25$ mm (which is characteristic for the side-to-side distance between bees at the surface of the bee curtain) ranged from 78.86 ms for mere *bucket-bridging* ($v_{bb} = 0.317$ m/s) to 48.33 ms (Fig. 9C) for the combination of *bucket bridging* and *saltatoric* propagation Fig. 9A ($k_{sp} = 41.5\%$; $v_{sp} = 0.8$ m/s).

Directional control in shimmering

Theoretically, the simplest way of wave propagation is by spreading energy along a straight line by directed and non-stochastic processes. In shimmering, information is transferred by bridging information along chains of surface bees (in agreement with the *directed-trigger* hypothesis [7,9]), where both, the *focus bees* and their *trigger neighbours*, are aligned perpendicular to the extension of the wave front. Although directedness in propagation has adaptive importance for shimmering [6,9,11–13], only less than 5% of agent bees (e.g., under ${}^{f}R_tL$) contribute to wave propagation in the main direction of a wave [9]. The present study confirms this apparent conundrum. An in-depth analysis was conducted (Fig. 10) with the data from one selected wave propagation direction (${}^{f}R_tL$) to test if the data confirms the *directed-trigger hypothesis* [7,9].

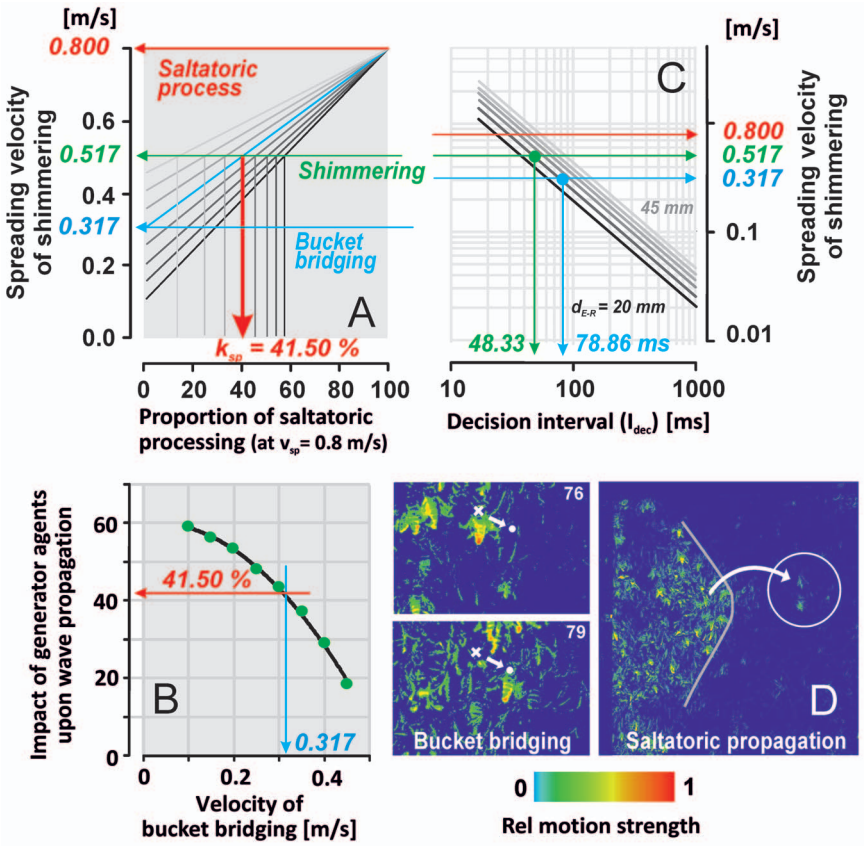

Figure 9. Mathematical model of the velocities in mixed-strategy wave propagation. (A) Lookup table for estimating the effect of the *saltatoric* process (sp) in shimmering in a mixed strategy with *bucket bridging* (bb): the proportion k_{sp} (abscissa) gives the impact of the *saltatoric* process on shimmering velocity (see Equations 3a,b) with v_{sh} as ordinate and with v_{sp} (= 0.8 m/s) and v_{bb} (= var [0.10–0.45 m/s]) as parameters. For the benchmark values (v_{sp} = 0.8 m/s; v_{bb} = 0.317 m/s; v_{sh} = 0.517 m/s) the impact of the *saltatoric* process on shimmering velocity is calculated as k_{sp} = 41.50%. (B) Ordinate, the impact of the *saltatoric* process on the empirical value of shimmering velocity (v_{sh} = 0.517 m/s) in dependence of *bucket bridging* (abscissa: v_{bb}) with the regression function: $k_{sp} = a \times v_{bb}^2 + b$ ($a = -97.57$, $b = 61.04$; v_{sp} = 0.8 m/s). (C) Lookup table to estimate the *decision interval* (abscissa: I_{dec} [ms]) of an agent bee in which she can decide to join a shimmering wave or not. I_{dec} is calculated as the time interval in which a wave front spreads from an emitter (E) bee to a receiver (R) bee; ordinate, shimmering velocity v_{sh} in m/s; the parameter d_{E-R} gives the distance between a *focus bee* and her adjacent neighbour (d_{E-R} = 20 to 45 mm). For a typical distance (d_{E-R} = 25 mm) the bee would have a time interval of I_{dec} = 48.33 ms to "decide" to join the wave (for v_{sh} = 0.517 m/s, green arrows); for the benchmark value of *bucket bridging* (v_{bb} = 0.317 m/s, blue arrows) this time interval would be longer (I_{dec} = 78.86 ms). (D) Pseudo coloured differential images (rel motion strength; see Figs. 1–2,4–5) to explain the principle of *bucket bridging* and of the *saltatoric* process.
doi:10.1371/journal.pone.0086315.g009

PEAK and SINK concepts. The *directed-trigger hypothesis* [7,9] predicts for every *focus bee* that their shimmering-active *neighbours* are distributed in angular sectors (α_{Nh}) of the *near neighbourhood* according to Equation 4.

$$P_{Nh}\ [\alpha_{Nh}] = {}^{rel}N_{nb} \times \sin^2(\alpha_{Nh}) \qquad (4)$$

where P_{Nh} is the probability of the occurrence of shimmering-active neighbours ($^{rel}N_{nb}$) of a *focus bee* at the respective angle α_{Nh} (for definition, see Fig. 10A).

The *directed-trigger hypothesis* postulates that in the *pre-stroke* phase of a *shimmering incident* the most shimmering-active neighbours ($^{rel}N_{nb}$) of *focus bees* are at the *ipsi-directional* side (where the wave is propagating from: see red arrows in Fig. 10A), and the least neighbours are present at the *contra-directional* side (where the wave is propagating to). For the *pre-stroke* phase, this hypothetical distribution of neighbours is described by Equations 5a,b and displayed in Fig. 10C_1,E_1, where blue curves show the maximal rates of shimmering neighbours $^{rel}N_{nb}$ at the *ipsi-directional* side defined by $\alpha_{Nh} \equiv \alpha_{WAV} = 0^\circ$ (under $dir_{WAV} = {}^{f}R_tL$). The distribution pattern shown in these curves is referred to as *PEAK* distribution pattern.

$$\min^{PEAK} P_{Nh} = P_{Nh}\ [\alpha_{Nh} \equiv 180^\circ] \qquad (5a)$$

$$\max^{PEAK} P_{Nh} = P_{Nh}\ [\alpha_{Nh} \equiv 0^\circ] \qquad (5b)$$

In the *post-stroke* phase, the hypothetical distribution of shimmering-active neighbours conforms to the *SINK* distribution pattern, with a maximum occurrence of $^{rel}N_{nb}$ at the *contra-directional* side, and a minimum occurrence of $^{rel}N_{nb}$ at the *ipsi-directional* side for $\alpha_{dirWAV} = 0^\circ$ (see Equations 6a,b; green curves in Fig. 10 D_1,F_1).

$$\min^{SINK} P_{Nh} = P_{Nh}\ [\alpha_{Nh} \equiv 0^\circ] \qquad (6a)$$

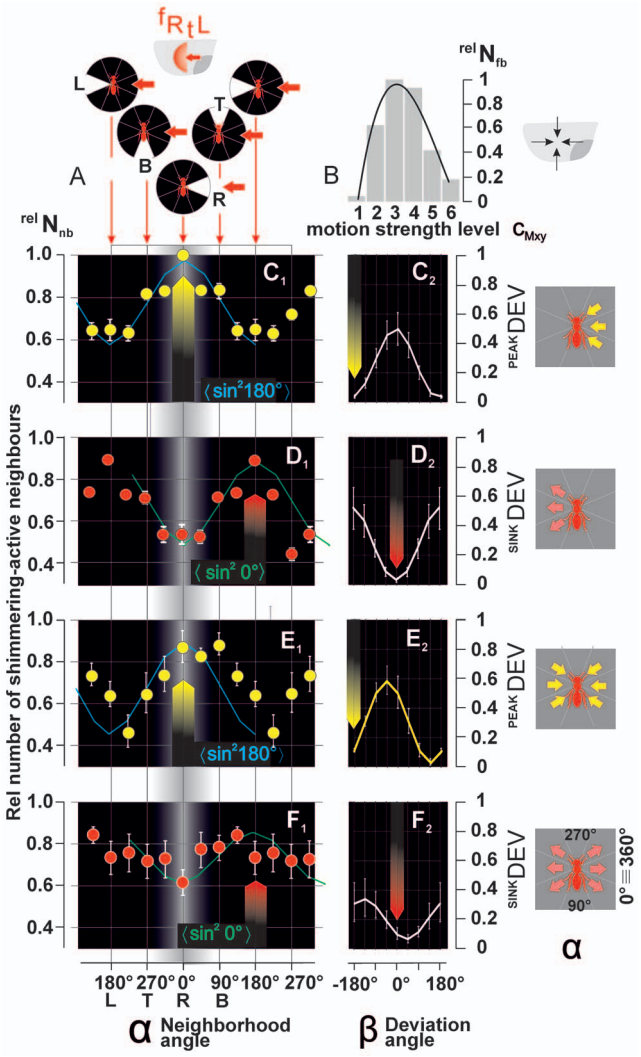

Figure 10. Directionality of status I–III agents. (A) Definitions: black circles indicate the *near neighbourhood* (<40 mm) with marked red *focus bees* in the centre; white angular sectors show the angles of neighbourhood (α_{Nh}, cf. Fig. 1C$_2$) as indicated by thin red vertical arrows and the corresponding abscissa of the panels C$_1$–F$_1$ regarding the directions *right* [R: $\alpha_{Nh}=0°$], *bottom* [B: 90°], *left* [L: 180°] and *top* [T: 270°]; thick red horizontal arrows indicate the direction of wave propagation, exemplified here for $dir_{WAV}={}^{f}R_tL$; (B) Histogram of *focus bees* (*status I–III*) of all wave directions ($dir_{all\ WAV}$: $N_{fb}=13{,}678$) in dependence of levels of motion strength (abscissa: $c_{Mxy}\in\{1..6\}$; for statistics, see Table S1). (C$_1$–F$_1$) Relative numbers of shimmering-active neighbours (ordinate: ${}^{rel}N_{nb}$ with $\max^{rel}N_{nb}=1.0$ per communication status) of *focus bees* in dependence of the neighbourhood angle (abscissa: α_{Nh}) and communication status (*status I*: C,D; *status II*: E, *status III*: F). Closed circles, arithmetic means; vertical bars, SEMs (n = 7 data sets of ${}^{f}R_tL$) give the neighbours that were shimmering-active prior to (yellow: panels C$_1$, E$_1$) and after (red: D$_1$, F$_1$) the t_0 of the abdominal flipping of the *focus bees*. Fitting functions (blue: *PEAK* distribution pattern; green: *SINK* pattern) give the occurrence of shimmering-active neighbour bees ($P_{Nh}[\alpha_{Nh}]$ as predicted by the *directed-trigger* hypothesis (see Equations 4–6). Upward red and yellow arrows point to the α_{Nh} values at which the maximal numbers of active neighbours are predicted. (C$_2$–F$_2$) *DEV* values (see Equations 8a,b) giving the deviation of the empirical ${}^{rel}N_{nb}$ values from the expected probability $P_{Nh}[\alpha_{Nh}+\beta]$ (Equation 7) with β as the deviation angle of the fitting function; white curves, means; vertical bars, SEMs. Downward arrows point to the α_{Nh} values at which the empirical distribution (${}^{rel}N_{nb}$) conforms to the *directed-trigger* hypothesis.
doi:10.1371/journal.pone.0086315.g010

$$\max^{SINK}P_{Nh}=P_{Nh}\ [\alpha_{Nh}\equiv 180°] \tag{6b}$$

Matching the empirical data with the hypothetical PEAK and SINK patterns

The empirical ${}^{rel}N_{nb}$ data were plotted against α_{Nh} and the resulting distributions compared with the hypothetical *PEAK* and *SINK* distribution patterns. ${}^{rel}N_{nb}$ data of all three agent types (*bucket bridging*, *chain-tail* and *generator* agents) were tested for correspondence with the hypothetical *PEAK* and *SINK* distribution patterns by cross-correlation according to Equation 7.

$$P_{Nh}\ [\alpha_{Nh}+\beta]={}^{rel}N_{nb}\times\sin^2(\alpha_{Nh}+\beta) \tag{7}$$

Here, the neighbourhood angle α_{Nh} (for definition, see Figs. 1C$_2$,10A) was altered by the deviation angle β in steps of 45° (with $-180°\leq\beta\leq+180°$) to identify the best match between the empirical data (displayed by full circles and vertical lines) and the *PEAK* and *SINK* curves. The hypothetical *PEAK* and *SINK* curves were normalized using the empirical differences between the $\min^{rel}N_{nb}$ and $\max^{rel}N_{nb}$ values for each agent type as reference (the normalized forms are indicated as $\{P_{Nh}\}$ The sums of the square differences between the ${}^{rel}N_{nb}$ values with the $\{P_{Nh}\}$ values were calculated for every angular step of neighbourhood $[\alpha_{Nh}+\beta]$ of the *focus bees*. The total deviation (*DEV*) over the total range of neighbourhood ($dir_{Nh}\in\{1..8\}$) between the empirical values (${}^{rel}N_{nb}$) and the normalized *PEAK* and *SINK* values were determined by Equations 8a,b.

$${}^{PEAK}DEV=\sqrt{\sum_1^8\{{}^{rel}N_{nb}-P_{Nh}\ [\alpha_{Nh}+{}^{PEAK}\beta]\}^2} \tag{8a}$$

$${}^{SINK}DEV=\sqrt{\sum_1^8\{{}^{rel}N_{nb}-P_{Nh}\ [\alpha_{Nh}+{}^{SINK}\beta]\}^2} \tag{8b}$$

with ${}^{PEAK}\beta=180°$ and ${}^{SINK}\beta=0°$.

Their reciprocal values constitute the goodness of the fit ${}^{PEAK}G$ and ${}^{SINK}G$ (Equations 9a,b) which can be tested using the χ^2-test.

$${}^{PEAK}G=G\ [\alpha_{Nh}+{}^{PEAK}\beta]=1/{}^{PEAK}DEV \tag{9a}$$

$${}^{SINK}G=G\ [\alpha_{Nh}+{}^{SINK}\beta]=1/{}^{SINK}DEV \tag{9b}$$

Furthermore, the probabilities ${}^{PEAK}P_m$ and ${}^{SINK}P_m$ for the match between the empirical data and the hypothetical *PEAK* and *SINK* distribution patterns was calculated according to Equations 10a,b, explaining the coincidence of the agents' directional properties with the *directed-trigger hypothesis*.

$${}^{PEAK}P_m=1-{}^{PEAK}DEV \tag{10a}$$

$${}^{SINK}P_m=1-{}^{SINK}DEV \tag{10b}$$

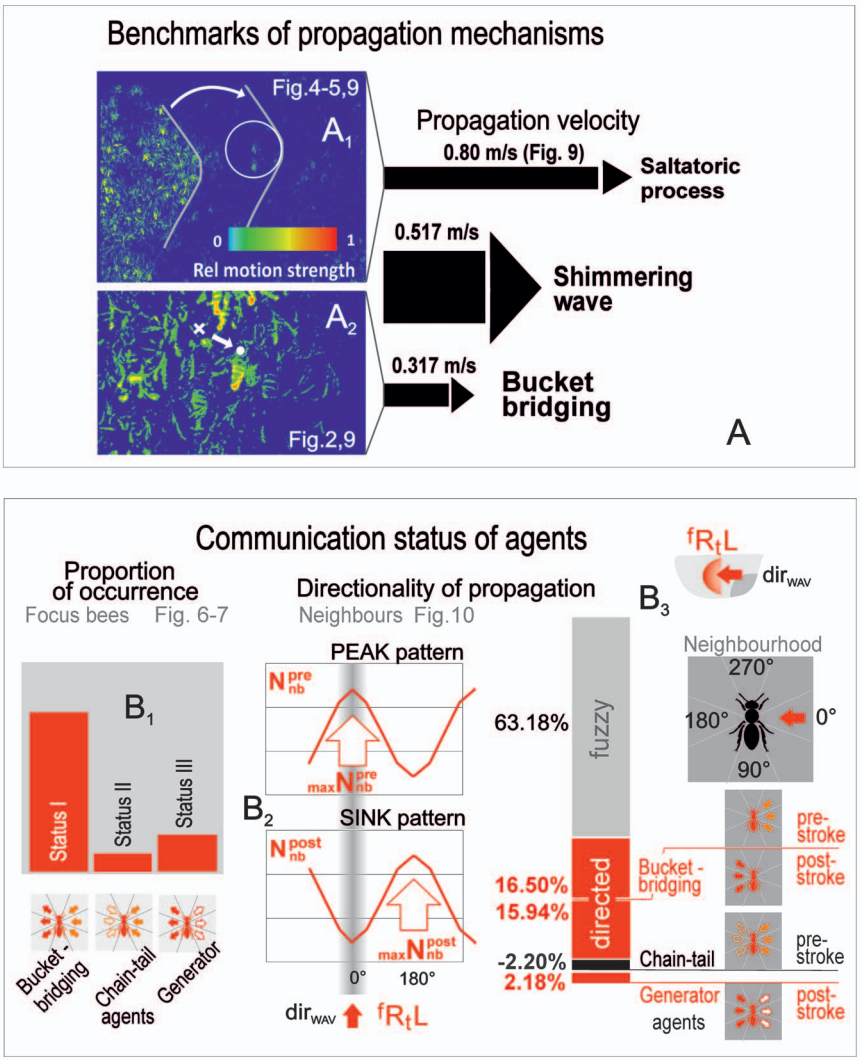

Figure 11. Summarization of results. (A) Assessment of benchmark values for both mechanisms of shimmering, the *saltatoric* wave propagation (panel A_1, cf. Figs. 4–5,9) and *bucket bridging* (panel A_2; Figs. 2,9). The lengths of the black arrows on the right side symbolize the propagation velocities of the partial processes (*saltatoric* processes and *bucket bridging*) and of *shimmering* as the mixed form of propagation. (B) Communication statuses of *focus bees* categorized in the *pre-stroke* and *post-*$[t_0]$*-stroke* phase by the recruitment level of their neighbours (nb), exemplified for the main wave direction $dir_{WAV} = {}^{f}R_tL$; B_1, the occurrence of the three types of agents (cf. Figs. 6–7); B_2, schematics of the angular ${}^{rel}N_{nb}^{pre}$ and ${}^{rel}N_{nb}^{post}$ distributions of shimmering-active neighbours (*PEAK* and *SINK* distribution pattern, cf. Fig. 10) addressing the match with the *directed-trigger* hypothesis; B_3, the impact of the three communication statuses on the control of directionality of the shimmering wave (cf. Fig. 10).
doi:10.1371/journal.pone.0086315.g011

The angular positions ($\alpha_{Nh}+\beta$), at which the *DEV* values exhibit a minimum (Fig. $10C_2$–F_2), represent the maximal goodness (*max G*) of the fit (Fig. $10C_1$–F_1). The resulting angular mismatch (MM) between the empirical data and the hypothetical *PEAK* and *SINK* distribution patterns was estimated by Equation 11, defined as the absolute deviation between the angle α^*_{Nh} (the angle with the minimum value of *PEAK* or *SINK* patterns, see Fig. 10 C_1–F_1), and β^*_{Nh} (the angle with the maximum goodness of the fit, see Fig. 10 C_2–F_2).

$$\Theta_{MM} = |\alpha^*_{Nh} - \beta^*_{Nh}| \qquad (11)$$

Lastly, the level E_{dirWAV} by which the different agent types contributed to the propagation of the main wave direction was estimated according to Equation 12.

$$E_{dirWAV} = {}^{rel}N_{nb} \times {}_{\max-\min}{}^{rel}\Delta N_{nb} \times P_m \times f_r \qquad (12)$$

where ${}^{rel}N_{nb}$ is the occurrence of shimmering-active neighbours of a *focus bee* in her *near neighbourhood*; ${}_{\max-\min}{}^{rel}\Delta N_{nb}$ is the percentage of active neighbours in defined α_{Nh} angles between maximal and minimal occurrences of ${}^{rel}N_{nb}$; P_m is the probability for the match between the empirical data and the hypothetical *PEAK* or *SINK* distribution patterns (Equations 10a,b); f_R is the reinforcement factor with $f_R = +1$ when the main wave direction is reinforced and $f_R = -1$ when the main wave direction is restrained.

Matching bucket-bridging agents. The *bucket-bridging* agents conformed to the *directed-trigger hypothesis* under *pre-stroke* and *post-stroke* conditions (Fig. 10 C_1–D_1) in different ways: the shimmering-active neighbours in the *pre-stroke* phase matched the *PEAK* distribution pattern four times more likely

($^{PEAK}P_G = 0.0061$, χ^2-test) than the *SINK* distribution pattern (Fig. 10 C_{1-2}; Table S2: $^{PEAK}DEV = 5.39\%$; $^{SINK}DEV = 19.28\%$; $^{PEAK}G = 18.54$; $^{SINK}G = 5.19$; $^{PEAK}\Theta_{MM} = 0^\circ$) and the factors calculated from equation 8 were $^{rel}N_{nb} = 0.4716$; $_{\max-\min}^{rel}\Delta N_{nb} = 0.3697$; $^{PEAK}P_m = 0.9461$; $f_R = +1$). Conversely, in the *post-stroke* phase the shimmering-active neighbours matched the *SINK* distribution pattern rather than the *PEAK* distribution pattern (Fig. 10 D_{1-2}, Table S2: $^{PEAK}DEV = 19.20\%$; $^{SINK}DEV = 4.57\%$; $^{PEAK}G = 5.21$; $^{SINK}G = 21.87$, $^{PEAK}P_G = 0.0014$, χ^2-test; $^{SINK}\Theta_{MM} = 0^\circ$). The factors calculated from equation 8 were $^{rel}N_{nb} = 0.4101$; $_{\max-\min}^{rel}\Delta N_{nb} = 0.4073$; $^{SINK}P_m = 0.9543$; $f_R = +1$. The total estimate of the influence of *bucket-bridging* agents to contribute to the wave propagation in the main shimmering direction was 32.44%, by adding up the E_{fRtL} value in the *pre-stroke* phase (16.50%) and that in the *post-stroke* phase (15.94%; Fig. 11B, Table S2).

Matching chain-tail agents. The angular distribution of shimmering-active neighbours of the *chain-tail* agents agreed stronger with the *PEAK* than the *SINK* distribution pattern ($^{PEAK}DEV = 9.23\%$; $^{SINK}DEV = 20.04\%$; $^{PEAK}G = 10.83$; $^{SINK}G = 4.99$; $P_{DEV} = 0.0459$, $^{PEAK}P_G = 0.1421$, χ^2-test; Fig. 10 E_{1-2}, Table S3), showing a small mismatch with the *PEAK*-pattern (Fig. 10E: $^{PEAK}\Theta_{MM} = 45^\circ$ ($\alpha^*_{Nh} = 180^\circ$, $\beta^*_{Nh} = 135^\circ$). This result shows that *chain-tail* agents can be identified by their match with the *PEAK* distribution pattern in the *pre-stroke* phase, and as they are the last agents in a chain they are the components that terminate the chain. Their contribution to shimmering ($E_{fRtL} = -2.20\%$) can be considered as constraining the wave propagation, which is noted by the negative value of f_R ($^{rel}N_{nb} = 0.0556$; $_{\max-\min}^{rel}\Delta N_{nb} = 0.4781$; $^{PEAK}P_m = 0.9077$; $f_R = -1$; Fig. 11B, Table S3).

Matching generator agents. In their *post-stroke* phase, *generator* agents activate their neighbours. Their distribution pattern agreed twofold more with the *SINK* than the *PEAK* pattern ($^{SINK}DEV = 8.79\%$; $^{SINK}G = 11.38$; $^{PEAK}DEV = 15.61\%$; $^{PEAK}G = 6.40$; Table S4), although this difference was not significant ($P_{DEV} = 0.1669$, $^{SINK}P_G = 0.2380$, χ^2-test). There was a small mismatch with the *SINK* pattern ($^{SINK}\Theta_{MM} = 45^\circ$ [$\alpha^*_{Nh} = 0^\circ$, $\beta^*_{Nh} = 45^\circ$]; Fig. 10 F_{1-2}) and the reinforcement of the main direction ($dir_{WAV} = {}^fR_tL$) was $E_{fRtL} = 2.1793\%$; $^{rel}N_{nb} = 0.0675$; $_{\max-\min}^{rel}\Delta N_{nb} = 0.3538$; $^{SINK}P_m = 0.9121$; $f_R = +1$; Fig. 11B, Table S4).

Discussion

Applying swarm models to giant honeybees

Shimmering in giant honeybees [1–9,11–14] is an intricate communication behaviour based on *swarm intelligence* [18–20] with *emergent* [20–23] social waves. The term *swarm* [24–26] is used for the ability of aggregations of similar morphological units to self-organize [19–22], form patterns, store information, and reach collective decisions [26–28]. *Swarms* display fluidity and uniformity in response, which emerge in dynamic behavioural patterns, such as in fish schools [26–28], in the fast ephemeral rolling patterns of starlings flocks (in particular under predation by falcons or gulls [24,29]), in the huddles of emperor penguins [30] or in groups of moving mammals [28,31]. The simplest mathematical model of an animal *swarm* defines individual agents with a Lagrangian approach [24,31–32], which have a gradient of repulsion and alignment around them following three rules: (a) *move in the same direction as your neighbours*, (b) *remain close to your neighbours*, and (c) *avoid collisions with your neighbours*. However, shimmering in giant honeybees does not match this *swarm* model: shimmering-active bees do not change their relative position in the bee curtain, and they move only parts of their body (Movies S1, S2, S3; [12]), although with the potential to generate directed moving patterns.

Stigmergy [34–35] (for summary and a broader definition see [36]) is another concept that may also help understanding the interaction between individual agents in shimmering. *Stigmergic* coordination stimulates behavioural responses through *traces* left in the environment. A shimmering wave affects all layers of the bee curtain mechanically [5,7–8,12] within tens of milliseconds (which can be considered as *traces*), thereby stimulating quiescent agent bees [7,9] to join the wave.

For the analysis of shimmering, concentric zones of *neighbourhood* were implemented around each *focus bee*, similar to the Lagrangian swarm models [25,32–33]. This concept allows the assessment of topological properties (cf. [37]) of the neighbours, such as the coordinates of the thoraces, and the strength and time of participation in the wave. Around 70% of shimmering-active bees (Fig. $7A_{1-2}$, *Status I*) act in a *bucket bridging*-like manner [9] while 88% of their immediate neighbours are also active (in the *pre-stroke* and *post-stroke* phases of *shimmering incidents*: Fig. $7A_3$, *Status I*). These agents contribute to the wave propagation in response to this mechanical commotion which mainly occurred in their *ipsi-directional* neighbourhood (where the wave came from). Their action also includes the release of Nasonov pheromone [38] that motivates defensive cohorts to stay rather than fly off and attack the enemy. They also stimulate their neighbours at their *contra-directional* side (towards which the wave is propagating) to join the abdominal flipping (Fig. $7C_{1,2}$, *Status I*).

On the other hand, a minority of about 15% (Fig. $7A_1$, *Status III*) of shimmering-active bees contribute to *saltatoric* wave propagation, and stimulate 6% (Fig. $7A_3$, *Status III*) of their neighbours to flip the abdomens. These *generator* agents start abdominal flipping before any *bucket-bridging* activity can be detected in their *near neighbourhood*, independent of the length of the discrimination window of <10 ff (Fig. $7B_3$). *Generator* agents are not prompted by their neighbours and therefore, have a lead role in decision-making by processing the visual cues of the threats, such as wasps in front of the nest, generating *daughter* waves. A *daughter* wave can merge with the steadily proceeding *parental* wave, forming a new wave front distally to the former *parental* wave front. Thus, the resulting *saltatoric* wave propagation is based on visual control which adds two new properties to the shimmering process [6]: it speeds up the wave front by a factor of up to three and allows the wave front to change direction rapidly with the potential that shimmering may even "follow" a threatening cue topologically on the nest (see Movies in [6,39]).

Goals of social waves

Social waves are hallmarks of animal aggregations. Besides giant honeybees, which display shimmering waves in response to wasps, birds and mammals [4–6,12], social waves have also been described for avian flocks [24,29,37,40–45], for the huddles of Emperor penguins [30], and for aggregations of humans in football stadiums [15]. A main question concerning social waves is whether they are advantageous for the aggregation, having received evolutionary function and conveying fitness benefits, or alternatively, whether they are simply a mere epiphenomenon of reactivity [43]. In the following, this question is discussed comparing the ephemeral rolling patterns in starlings and the shimmering waves in giant honeybees.

Waves in starling flocks. Starlings form flocks especially before they roost, to effectively maintain cohesion of the group, strongly supporting survival [37,41–42]. Under predation they

display spectacular ephemeral rolling patterns. Individual starlings may be kept informed in the flock about the progress and the state of such an ongoing "wave" by continuous inspection from the momentary vantage point. In reality, this information is restricted to a topological group of 6–7 neighbours [37]. Although an individual starling has some room to modify its decision to participate in the concerted flight manoeuvre, it cannot decline to conjointly move together with its neighbours. This constraint is less due to the potential danger of being eaten by the predator [29] but more due to the danger of collision [37,41–42]. These rolling patterns display trains of pulses of optical density that propagate across the flock and are produced within the swarm body, mostly without affecting the swarm surface. The authors explain [29] that such pulses are formed in proximity to the bird of prey, mostly laterally, and are propagated typically away from it. These patterns may lead to *confusion* [6,46] of the predator and encounter *dilution* [47] but the cause for their evolution is only poorly understood.

Shimmering waves. The goals of shimmering [5–13] in giant honeybees differ from the rolling waves of starling flocks [29,37,41–42] in the following ways: Shimmering waves are produced by stationary agents (Movies S1, S2, S3, S4, S5, S6). Most of the colony members, including those in subsurface layers or at the opposite comb side, continually receive information about the shimmering status mechanoceptically [7–8,12]. Surface bees also release Nasonov pheromone [38], motivating others to participate in the wave. Shimmering giant honeybees may or may not join the wave, and if they join, they can determine when to start their contribution and at which strength [7,9]. Both, starlings and giant honeybees have the potential to respond rapidly to changing visual cues, and in both cases directivity seems to be strongly controlled.

In giant honeybees, the directivity of *bucket bridging* was described previously [8]. In the present work, we show that the majority of shimmering-active bees (63.18%) do not contribute to the wave propagation in the main direction (Fig. $11B_3$). Of the other 36.82% of the shimmering-active bees which contribute to the directional control, 88.09% are *bucket-bridging* agents, 5.98% are *chain-tail* agents and 5.92% are *generator* agents (Table S2, S3, S4). *Generator* agents are less affected by the oncoming wave than the two other agent types (Fig. $7B_3$,10F), contributing less, and fuzzily, to wave direction control. This fuzziness of *generator* agents is important, because it enables rapid changes in wave direction in response to rapidly moving cues (cf. [39]).

Why do giant honeybees speed up shimmering waves?

Taken together, the aspects discussed above appear to contribute to the *confusion* and *repellence* of predators [6,12,39], but they cannot explain why *saltatoric* propagation has evolved. Three possible explanations for this conundrum are discussed below: *saltatoric* propagation could reinforce (a) the recruitment of shimmering agents, (b) the repelling effect on predating wasps by directed visual patterns and (c) the *bottom-up* attention in vertebrate predators.

Saltatoric propagation reinforces recruitment. More agents are recruited when shimmering is accelerated above the "base" speed of *bucket bridging* ($v_{bb} = 0.317$ m/s) by *saltatoric* propagation ($v_{sp} = 0.517$ m/s) than during *bucket bridging* alone (Figs. 1–2,3–4,9). This increased recruitment is due to the generation of *daughter* waves, causing rapid, exponential growth of the visual pattern with a concomitantly greater repelling effect, which likely benefits the giant honeybee colony. This explanation is in agreement with previous findings [6] that more bees contribute to shimmering the faster and the nearer to the bee nest a preying wasp flies.

Saltatoric propagation increases the repelling effect on predating wasps by directed visual patterns. Giant honeybees have the capability to align the direction of their shimmering waves with the flight path of a preying wasp [6,39]. In this prey-predator interaction both, the bees and the wasp emit signals and both respond to stimuli of their counterparts, whereby the honeybees can change the direction of their shimmering waves faster than the wasps can turn [39]. This asymmetry between bee and wasp is based upon the greater speed of wave propagation and the fuzziness in directional control by *saltatoric* propagation.

Saltatoric propagation may reinforce bottom-up attention in vertebrates. Giant honeybees display shimmering in response to wasps, but also to birds and mammals that approach the nest within distances of about 3 m (own observations). Shimmering produces repetitively moving circular areas, typically with a diameter of 20 cm or more. Mammals and birds may perceive these patterns as supernormal cues that represent moving, head-like structures [48], outwitting their perceptual systems. Such cues may release a startle response [48–49] in vertebrates based on *bottom up* (BU) attention [50–53]. *Bottom up* attention depends upon the properties of a sensory stimulus to capture full attention, such as a bright spot of colour, an area of sharp contrast, or a rapidly moving pattern, such as typically involved in shimmering [1–13].

In higher vertebrates, the retinal fovea is the main sensory interface for attention retrieval [50–51]. When a shimmering wave is imaged by the fovea under *covert* conditions (with fixated eyes), BU attention is likely stronger the greater the image of the shimmering wave is, until the image fully covers the fovea. The fovea receptors are most densely packed in the central 1–2°, and the maximal trace length of a moving object that crosses a central projection at the main acuity region of the fovea is less than 10° [50–51]. The trace length of a shimmering wave on a vertebrate fovea in the 200 ms of the *ascending* phase (Fig. 3B, [6]) will cover an angle of 10°, provided that circular patterns of 20 cm or more are produced and viewed from a distance of 1 m from the nest. In the *climax* phase of a shimmering wave (Fig. 3B), when the patterns move at a speed of $v_{sh} = 0.514$ m/s (Fig. 9A) they will be viewed with a foveal path length of 8.154°, whereas mere *bucket-bridging* propagation ($v_{bb} = 0.325$ m/s) will affect only a path length of 5.400°.

Summary and Conclusions

Characteristics and benchmark data of two propagation mechanisms (Fig. 11A) of shimmering, *bucket bridging* and the *saltatoric* processes were investigated. Combining both mechanisms speeds up the shimmering waves from 0.317 m/s (*bucket bridging* only) to 0.517 m/s, which shows that the *saltatoric* component, also associated with the generation of *daughter* waves, increases the overall propagation speed of shimmering by 40%. Three categories of shimmering-active surface bees were identified regarding their communication status: the *bucket-bridging*, *chain-tail* and *generator* agents. These agents comprise a characteristic proportion (Fig. $11B_1$) and a characteristic recruitment status with respect to their neighbours (Fig. $11B_2$), and they contribute differently to the directivity of the main shimmering wave (Fig. $11B_3$). Summarizing, the wave-like shimmering process in giant honeybees displays adaptive complexity, particularly regarding the generation and propagation of information, and is an impressive example of swarm intelligence [19–21]. Shimmering conforms to rules of *bucket-bridging* such as *linearity*, *continuity* and *graduality* [9] and involves an additional *saltatoric* strategy to speed

up signal transmission, but also to provide a high level of fuzziness (Fig. 11B_3) which may enable giant honeybee colonies to respond to rapidly changing threats [39].

Supporting Information

Glossary S1 List of important terms, definitions and abbreviations used in this paper.
(DOCX)

Movie S1 In this episode two successive waves were generated by a dummy wasp that was moved from left to right (in the image). The episode started at f 1, but the playback session refers only to ff 550–650 (corresponding to 1,700 ms). The dummy wasp was moved 20 cm in front of the nest (shown at the left bottom corner of the image). The part of the nest displayed in the film corresponded to the area marked by the four yellow spots in Fig. 1A and comprised about 1,250 bees of the surface layer; the thorax of the *focus bee* selected for this film was marked in red. Left panel: black-and-white images, inverted to enhance the contrast of the abdomens; right panel: the same view but displayed as differential image with the motion strength in pseudo colours (with relative motion strength scaled from *blue* = 0.0 to *red* = 1.0; see rainbow scale on the right bottom side). Original recording speed: fps = 60 Hz; playback speed: fps = 60 Hz.
(AVI)

Movie S2 The same episode as in Movie S1, but zoomed for about 60 bees; original recording speed: fps = 60 Hz; playback speed: fps = 60 Hz.
(AVI)

Movie S3 The same episode as in Movie S1, playback speed: fps = 25 Hz (slow motion factor: 0.42 of original speed).
(AVI)

Movie S4 The same episode as in Movie S2, but with a playback speed of fps = 25 Hz as in Movie S3.
(AVI)

Movie S5 The same episode as in Movie S1, but with a playback speed of fps = 6 Hz (slow motion factor: 0.10 of original speed)
(AVI)

Movie S6 The same episode as in Movie S2, but with a playback speed of fps = 6 Hz as in Movie S5.
(AVI)

Table S1 Accessory table to the Fig. 7 B–C, Fig. 8 A–C and Fig. 10 B with details of the regression functions regarding individual bees on the surface of the experimental giant honeybee nest B identified as *status I–III* agents (for definition, see text); tw, time window in [ff] at fps = 60 Hz; $_{all}$dir, all four main directions of the spreading of the shimmering waves as selected in the paper: $^{f}R_tL$, $^{f}L_tR$, $^{f}T_tB$, $^{f}B_tT$; with *R,L,T,B* as *right*, *left*, *top*, *bottom*; abscissa and ordinate, the parameters used in the respective Figures/panels; coefficients of regressions (polynomials, exponential functions) are not detailed here; *number of cases* gives the number of *focus* bees or *neighbour* bees as evaluated in the data sets; *goodness of fit* (R^2) regards the regression functions of mean values.
(DOCX)

Table S2 Survey of the data associated to Figs. 7,10 concerning agents of the *bucket-bridging* (*Status I*) type; experimental nest B (see Methods); [a,b], significant differences ($P_{DEV}<0.01$, χ^2 test) within groups. The *hypothetical distributions* are normalized denotations of *PEAK* and *SINK* distribution patterns (see Results).
(DOCX)

Table S3 Survey of the data associated to Figs. 7,10 concerning agents of the *chain-tail* (*Status II*) type; experimental nest B (see Methods); [a] significant differences ($P_{DEV} = 0.0459$, χ^2 test) within groups; na, not available data; the *hypothetical distributions* are normalized denotations of *PEAK* and *SINK* distribution patterns (see Results).
(DOCX)

Table S4 Survey of the data associated to Figs. 7,10, concerning agents of the *generator* (*Status III*) type; experimental nest B (see Methods); [a] non-significant differences ($P_{DEV} = 0.1669$, χ^2 test) within groups; na, not available data; the *hypothetical distributions* are normalized denotations of *PEAK* and *SINK* distribution patterns (see Results).
(DOCX)

Acknowledgments

We thank Dr. Madhu Singh, Dr. S.M. Man, Dr. R. Thapa and Dr. M. B. Gewali from the Tribhuvan University, Kathmandu, for their support regarding logistics, Klaus Maresch, Bonn for help with handling of the bees in Chitwan, and Horst Bischof and Mathias Rüther of the Technical University of Graz, Austria, for support with the development of the specific software used in this study.

Author Contributions

Conceived and designed the experiments: GK TH FW. Performed the experiments: FW TH MM GK. Analyzed the data: GK FW TH SW MM. Contributed reagents/materials/analysis tools: GK FW TH MM. Wrote the paper: GK IK.

References

1. Roepke W (1930) Beobachtungen an indischen Honigbienen, insbesondere an *Apis dorsata*. Meded LandbHoogesch Wageningen, 34: 1–28.
2. Butler CG (1954) The world of the honeybee. London.
3. Lindauer M (1956) Über die Verständigung bei indischen Bienen. Z Vergl Physiol 38: 521–557.
4. Seeley TD, Seeley RH, Aratanakul P (1982) Colony defence strategies of the honeybees in Thailand. Ecological monographs 52: 43–63.
5. Kastberger G (1999) The magic trees of Assam – Documentary film about the biology of the giant honeybee *Apis dorsata*. National Geographic, ZDF, ORF & epo-film, ,Wien.
6. Kastberger G, Schmelzer E, Kranner I (2008) Social waves in Giant honeybees repel hornets. PLoS ONE, 3(9): e3141. doi:10.1371/journal.pone.0003141.
7. Kastberger G, Maurer M, Weihmann F, Ruether M, Hoetzl T et al. (2011) Stereoscopic motion analysis in densely packed clusters: 3D analysis of the shimmering behaviour in Giant honey bees. Frontiers in Zoology, 8: 3. doi: 10.1186/1742-9994-8-3.
8. Kastberger G, Weihmann F, Hoetzl T (2013) Social waves in giant honeybees (*Apis dorsata*) elicit nest vibrations. Naturwissenschaften 100: 595–609. doi: 10.1007/s00114-013-1056-z.
9. Kastberger G, Weihmann F, Hoetzl T, Weiss SE, Maurer M (2012): How to Join a Wave: Decision-Making Processes in Shimmering Behavior of Giant Honeybees (*Apis dorsata*). PLoS ONE, 7(5): e36736. doi:10.1371/journal.pone.0036736.
10. Morse RA, Laigo FM (1969) *Apis dorsata* in the Philippines. Philipp Assoc Ent 1: 1–96.
11. Schmelzer E, Kastberger G (2009) "Special agents" trigger social waves in Giant honeybees (*Apis dorsata*). Naturwissenschaften, 96:1431–1441.
12. Kastberger G, Weihmann F, Hoetzl T (2011) Self-Assembly Processes in Honeybees: The Phenomenon of Shimmering. In: Honeybees of Asia, Hepburn R, Radcliff S (eds), Chapter 18. ISBN: 978-3-642-16421-7 (Print) 978-3-642-16422-4 (Online).
13. Weihmann F, Hoetzl T, Kastberger G (2012) Training for defence? From stochastic traits to synchrony in Giant honeybees (*Apis dorsata*). Insects, 3(3): 789–820. doi:10.3390/insects3030789.
14. Woyke J, Wilde J, Wilde M (2008) Comparison of Defense Body Movements of *Apis laboriosa*, *Apis dorsata dorsata* and *Apis dorsata breviligula* Honey Bees. J Insect Behav 21:481–494.

15. Farkas ID, Helbing D, Vicsek T (2002) Social behaviour: Mexican waves in an excitable medium. Nature, 419:131–132. doi:10.1038/419131a.
16. Phillips OM (1977) The dynamics of the upper ocean. Cambridge University Press, USA.
17. Holthuijsen LH (2007) Waves in oceanic and coastal waters. Cambridge: Cambridge University Press.
18. Camazine S, Deneubourg JL, Franks NR, Sneyd J, Theraulaz G, et al. (2003) Self-organization in biological systems. Princeton University Press, Princeton.
19. Beni G, Wang J (1989) Swarm Intelligence in Cellular Robotic Systems. Proceed NATO Advanced Workshop on Robots and Biological Systems, Tuscany, Italy.
20. Bonabeau E, Dorigo M, Theraulaz G (1999) Swarm Intelligence: From Natural to Artificial Systems. Oxford University Press, Inc. New York, NY, USA, ISBN 0-19-513159-2,
21. Kauffman S (1993) The Origins of Order: Self-Organization and Selection in Evolution. Oxford University Press, ISBN 0-19-507951-5,.
22. Goodwin B (2001) How the Leopard Changed Its Spots. The Evolution of Complexity. Princeton University Press.
23. Johnson SB: Emergence (2001) The Connected Lives of Ants, Brains, Cities, and Software. Scribner's, ISBN 0-684-86876-8.
24. Hildenbrandt H, Carere C, Hemelrijk CK (2010) Self-organized aerial displays of thousands of starlings: a model. Behav Ecol 21, 1349–1359. doi:10.1093/beheco/arq149.
25. Reynolds CW (1987) Flocks, herds and schools. A distributed behavioral model. Computer Graphics 21 (4): 25–34. doi:10.1145/37401.37406. ISBN 0-89791-227-6.
26. Parrish JK, Viscido SV (2005) Traffic rules of fish schools: a review of agent-based approaches. In: Self-Organisation and the Evolution of Social Behaviour, Hemelrijk CK (ed). Cambridge University Press.
27. Gerlotto F, Bertrand S, Bez N, Gutierrez M (2006) Waves of agitation inside anchovy schools observed with multibeam sonar: a way to transmit information in response to predation. ICES Journal of Marine Science 63: 1405–1417.
28. Couzin ID, Krause J (2003) Self-organization and collective behaviour in vertebrates. Advances in the Study of Behavior 32 :1–75.
29. Procaccini A, Orlandi A, Cavagna A, Giardina I, Zoratto F, et al. (2011) Propagating waves in starling, *Sturnus vulgaris*, flocks under predation. Animal Behaviour 82:759–765.
30. Zitterbart DP, Wienecke B, Butler JP, Fabry B (2011) Coordinated Movements Prevent Jamming in an Emperor Penguin Huddle. PLoS ONE, 6(6): e20260. doi:10.1371/journal.pone.0020260.
31. Couzin ID, Krause J, Franks NR, Levin SA (2005) Effective leadership and decision-making in animal groups on the move. Nature 433:513–516.
32. Virmani S, Adrian EC, Imhof K, Mukherjee S (1989) Implementation of a Lagrangian relaxation based unit commitment problem. IEEE Trans Power Syst 4(4): 373–1380.
33. An G, Mi Q, Dutta-Moscato J, Vodovotz Y (2009) Agent-based models in translational systems biology. Systems Biology and Medicine 1: 159–171; doi:10.1002/wsbm.45.
34. Grasse P (1959) La reconstruction du nid et les coordinations inter-individuelles chez Bellicostitermes natalensis et Cubitermes . sp. La theorie de la stigmergie: Essai d'interpretation du comportement des termites constructeurs. Insectes Sociaux 61:41–80.
35. Mason Z (2002): Programming with Stigmergy: Using Swarms for Construction. In: Artificial Life VIII, Standish, Abbass, Bedau (eds), MIT Press 371–374.
36. Small P (2003) Stigmergic systems. http://www.stigmergicsystems.com/stig_v1/stigrefs/article1.html?540817.
37. Ballerini M, Cabibbo N, Candelier R, Cavagna A, Cisbani E, et al. (2008) Interaction ruling animal collective behavior depends on topological rather than metric distance: Evidence from a field study. PNAS105:1232–1237.
38. Kastberger G, Raspotnig G, Biswas S, Winder O (1998) Evidence of Nasonov scenting in colony defence of the Giant honeybee *Apis dorsata*. Ethology 104: 27–37.
39. Kastberger G, Weihmann F, Zierler M, Hoetzl T (2013) Wasps Giant honeybees (*Apis dorsata*) mob wasps away from the nest by directed visual patterns. Naturwissenschaften, submitted.
40. Potts WK (1984) The chorus-line hypothesis of manoeuvre coordination in avian flocks. Nature 309: 344–345.
41. Ballerini M, Cabibbo N, Candelier R, Cavagna A, Cisbani E, et al. (2011) Empirical investigation of starling flocks: a benchmark study in collective animal behaviour. Animal Behaviour 76:201–215.
42. Cressey D (2011) Starling waves help flocks flummox falcons. Nature News Blog, http://blogs.nature.com/news/2011/08/starling_waves_help_flocks_fox.html
43. Parrish JK, Edelstein-Keshet L (1999) Complexity, Pattern, and Evolutionary Trade-Offs in Animal Aggregation. Science, 284: 99–101.Winter D: Winter starlings on Otmoor. http://www.youtube.com/watch?v = XH-groCeKbE, uploaded 21.02.2007.
44. Hoffmann T (2011) Spreeuwenspektakel Hoograven Utrecht http://www.youtube.com/watch?feature = player_detailpage&v = _tEFRAI9WSE, uploaded 03.03.2011.
45. Downer J (2012) Peregrine Falcon Hunts Starlings in Rome: http://www.youtube.com/watch?feature = player_detailpage&v = V-mCuFYfJdI, uploaded 11.01.2012.
46. Landeau L, Terborgh J (1986) Oddity and the 'confusion effect' in predation. Animal Behaviour 34, 1372–1380.
47. Hamilton WD (1971) Geometry for the selfish herd. J Theor Biology 31, 295–311.
48. Alcock J (2005) Animal Behaviour. Sinauer Associates inc, Massachusetts, Eight edition 2005.
49. Zupanc GKH (2010) Behavioral Neurobiology: An Integrative Approach. Foreword by Theodore H. Bullock. Second Edition. ISBN 978-0-19-920830-2. Oxford University Press.
50. Itti L, Gold C, Koch C (2001) Visual Attention and Target Detection in Cluttered Natural Scenes. Optical Engineering 40(9):1784–1793.
51. Droll JA (2011) Think Fast! The Velocity of Visual Attention in Vehicle Accidents. American Association for Justice, MEA Forensic Engineers & Scientists Inc., Motor Vehicle Section 17 (2).
52. Simons DJ, Chabris CF (1999) Gorillas in our midst: Sustained in attentional blindness for dynamic events. Perception 28:1059–1074.
53. Olson PL (1996) Forensic aspects of driver perception and response. Tucson, AZ: Lawyers & Judges Publishing Company, Inc.